The role of Southern Hemispheric Westerlies for Holocene hydroclimatic changes in the steppe of Tierra del Fuego (Argentina)

Cecilia Laprida, María Julia Orgeira, Marilén Fernández, Rita Tófalo, Josefina Ramón Mercau, Gabriel E. Silvestri, Ana Laura Berman, Natalia García Chapori, María Sofía Plastani, Susana Alonso

PII: S1040-6182(20)30616-9

DOI: https://doi.org/10.1016/j.quaint.2020.09.051

Reference: JQI 8541

To appear in: *Quaternary International*

Received Date: 3 June 2020

Revised Date: 28 September 2020

Accepted Date: 29 September 2020

The role of Southern Hemispheric Westerlies for Holocene hydroclimatic changes in the steppe of Tierra del Fuego (Argentina)

Cecilia Laprida[1], María Julia Orgeira[2], Marilén Fernández[3], Rita Tófalo[2], Josefina Ramón Mercau[1], Gabriel E. Silvestri[4], Ana Laura Berman[4], Natalia García Chapori[1], María Sofía Plastani[5] and Susana Alonso[2]

[1]: Instituto de Estudios Andinos Don Pablo Groeber. Facultad de Ciencias Exactas y Naturales, Universidad de Buenos Aires. Avenida Intendente Güiraldes 2160, Ciudad Universitaria, C1428EGA, Ciudad Autónoma de Buenos Aires, Argentina. chechulaprida@gmail.com; m.josefina.ramon@gmail.com; natalia.garcia.chapori@gmail.com.

[2]: Instituto de Geociencias Básicas, Aplicadas y Ambientales de Buenos Aires. Avenida Intendente Güiraldes 2160, Pabellón II, Piso 1, Ciudad Universitaria, C1428EGA, Ciudad Autónoma de Buenos Aires, Argentina. mjorgeira@yahoo.com.ar; tofalo@gl.fcen.uba.ar; alonso.msusana@gmail.com, maria julia Orgeira.

[3]: Centro Austral de Investigaciones Científicas. Bernardo Houssay 200, Ushuaia, Tierra del Fuego, Argentina. Shanamain@gmail.com.

[4]: Centro de Investigaciones del Mar y la Atmósfera. Departamento de Ciencias de la Atmósfera y los Océanos. C. Universitaria, Pab. II. 2°piso. (1428) Buenos Aires. Argentina. splastani@gmail.comgabriel.emilio.silvestri@gmail.com; ana.laura.berman@gmail.com.

[5]. Departamento de Ciencias Geológicas. Facultad de Ciencias Exactas y Naturales, Universidad de Buenos Aires. Avenida Intendente Güiraldes 2160, Ciudad Universitaria, C1428EGA, Ciudad Autónoma de Buenos Aires, Argentina. splastani@gmail.com

Corresponding author: Cecilia Laprida

chechulaprida@gmail.com

Instituto de Estudios Andinos "Don Pablo Groeber"

Facultad de Ciencias Exactas y Naturales - Universidad de Buenos Aires

Intendente Güiraldes 2160 - Ciudad Universitaria - Tel. (++54 +11) 5285-7400

C1428EGA -Ciudad Autónoma de Buenos Aires - Argentina

Abstract

The steppe of northern Tierra del Fuego is an important region for studying climate variability in the Southern Hemisphere, due to its position at the southern margin of the Southern Hemisphere Westerly Wind belt. Here we present a multiproxy analysis of a sedimentary sequence from Laguna Carmen (53°S, 68°W) which provides evidence of the progressive aridity and strengthening of the low-level Westerlies during the Late Holocene. We identified three prominent phases in the climatic record from Laguna Carmen: a cold and wet period between ~4000 cal. BP and ~2200 cal. BP, evidenced by a relative high lake level, periodic runoff into the lake, and oligohaline (mean: 2554 µS/cm) salinities; a step-change towards warmer and drier conditions after ~2200 cal. BP, reflected by limited runoff and oligo-mesohaline salinities (mean: 4799 µS/cm); and finally, the establishment of modern semi-arid conditions some time after ~1000 cal. BP, when the lake became a shallow lake that sometimes dried out during the summer. Our results coincide with paleoclimatic numerical models that suggest a progressive aridification of the southern Patagonian steppe since 6000 cal. BP due to stronger Westerlies and higher temperatures associated with changes in solar irradiance.

Keywords

Southern Hemisphere Westerly Winds, multiproxy analysis, lithofacies, hydrological balance, diatoms, ostracods.

1. Introduction

The belt of Southern Westerlies constitutes a distinctive feature of Southern Hemisphere atmospheric circulation south of 30°S with a significant influence on weather and climate at extratropical latitudes. Patagonia, the southernmost tip of South America, is the only continental landmass covering the core zone (~50°-55°S) of the low-level Westerlies (LLW) offering an ideal setting to examine patterns, } mechanisms and effects of (paleo)climate change on terrestrial environments.

Several climate reconstructions have suggested that latitudinal shifts and/or intensity variations of the LLW were the main drivers of regional climate and environmental change in Patagonia during the Late Quaternary (Whitlock et al., 2007; Mayr et al., 2007; Lamy et al., 2010; Zolitschka et al., 2013, 2018). Reconstructions often rely on modern relationships between zonal winds and precipitation, but they reach (partially) contradicting conclusions concerning strength and/or position of the LLW and their paleoclimatic implications (Kilian and Lamy, 2012). Some authors have proposed a strengthening of the westerly flow towards the Middle Holocene (Moreno et al., 2010; Fletcher and Moreno, 2011) for the LLW core region, while others concluded that there was a decrease in zonal wind intensity (Lamy et al., 2010). Moreover, Late Holocene climate variability in the southern Patagonian steppe is controversial since paleoenvironmental reconstruction is hindered by the relatively low number of available records (Kilian and Lamy, 2012), conflicting chronologies, spurious correlations between proxies and climatic parameters (Mayr et al., 2007), and the usually neglected effect of the surface wind speed changes on the hydrological balance (Lamy et al., 2010).

Aside from the LLW, the role of insolation as climate forcing parameter in Southern Patagonia during the Holocene has received little attention (Pérez-Rodríguez et al., 2016; Turney et al., 2016), probably because some authors suggested that the link between proxy data and insolation changes is not straightforward (Kilian and Lamy, 2012). However, the response of temperature, precipitation, and atmospheric circulation patterns to variations in the seasonal cycle of insolation was explored with different numerical models to investigate the evolution of regional paleoclimatic conditions in southern South America (Rojas and Moreno, 2011; Berman et al., 2017). Although these simulations are focused on specific time slices (Bracconot et al., 2012), model output provides valuable information to infer the past climate evolution in this region.

In the last few years, several studies were conducted for shallow lakes from northern Tierra del Fuego, the southern margin of the LLW (Fig. 1) (geological and geomorphological characterization, Orgeira et al., 2012, Coronato et al., 2017; morphometric and hydrological characteristics, Villarreal and Coronato, 2017; paleomagnetic secular variations, Gogorza et al., 2018; recognition of wet/dry intervals, Borromei et al., 2018, Last Glacial Maximum and Holocene hydrological evolution, Fernández et al., 2020). In shallow lakes of semi-arid regions, water balance is frequently reflected in the solute composition and salinity, which is one of the factors determining ostracod and diatom assemblages, allowing their use as proxies for (semi)quantitative environmental reconstructions (i.e. Ramón Mercau et al., 2012; Ramón Mercau and Laprida, 2016; Coviaga et al., 2017; Ohlendorf et al., 2014; Borromei et al., 2018). Additionally, and due to low precipitation and sparse vegetation cover of the soils in this region, grain size distribution and geochemical signatures of lacustrine sediments allow budgeting fluvial and aeolian sediment input. As such, both salinity and the regime of sediment input can be interpreted regarding lake level, sediment availability, and low-level atmospheric circulation patterns.

In this work we integrate selected biological (ostracods, diatoms), physical (sedimentology, mineralogy, magnetic susceptibility), and geochemical data (elemental analysis, total organic carbon, total inorganic carbon, total sulfur) from a sediment core of Laguna Carmen on the island of Tierra del Fuego, southernmost Patagonia, to detect temporal changes in local hydrological balance and define the sediment sources during the Late Holocene. Finally, we compare our results with other paleolimnological records of Southern Patagonia analyzing the spatial and temporal coherence in lake responses to large-scale driving forces.

2. Regional setting

Laguna Carmen (53°40'S, 68°18'W, 29 m asl) is a small pan (1.97 km^2) that bears a shallow lake less than 2 m-deep located in the northeastern Fuegian steppe, Southern Patagonia (Fig. 1). It is the depocenter of a closed basin (< 50 km^2) surrounded by low mountain ranges and isolated hills < 200 m high and dissected by fluvial erosion with a regional slope towards the northeast. The lake is normally frozen during winters, whereas it becomes sometimes dessicates during summers (Villarreal and Coronato, 2017). It is fed by several temporal streams fed by precipitation and snowmelt-derived runoff, most of which comes from the west (Coronato et al., 2017). The most important inflow runs through the northeastern slope of the Cerro Mesa (190 m asl), which is composed of fluvial sandstones and conglomerates of the Castillo Formation (Codignotto and Malumián, 1981). The lacustrine basin was formed by intense aeolian deflation of alluvial deposits during the Late Quaternary (Orgeira et al., 2012). Then, the area experienced conditions of higher humidity which resulted in episodes of higher-than-present lake levels, as evidenced by the presence of two lacustrine terraces at 34-35 and 30-31 m asl, at NW, S and SW shores, and an inactive outflow towards the east (Coronato et al., 2017). The lacustrine terraces were formed by wave action in hard rocks of the Miocene Carmen Silva Formation during higher-than-present lake levels (Coronato et al., 2017).Towards the NE of the lake, the presence of a large dune field migrating eastwards attests windy conditions that currently prevail.

The climate is semi-arid and cold/temperate, with significant influence from the South Pacific Anticyclone, which provides constant winds coming from the NW, W, and SW (Villarreal and

Coronato, 2017). Temperature is affected by two atmospheric patterns that produce marked variability at different time scales (Berman et al., 2013): anticyclonic (cyclonic) anomalies extending over southernmost South America and adjacent oceans reduce (increase) the cloud cover increasing (reducing) the solar heating that promotes warm (cold) conditions in the region; and cyclonic (anticyclonic) anomalies developed at subpolar latitudes hinder (favor) outbreaks of cold air increasing (decreasing) the temperature over southern Patagonia. The mean annual temperature is 5.5 °C. The mean temperature of the coldest month (August) has been established as -2 °C and of the warmest month (February) as 10 °C. Although monthly mean minimum temperatures frequently reach below the freezing point from May to September, they are usually higher than -3°C (Hoffman, 1975, Prohaska, 1976). Precipitation is distributed regularly throughout the year with annual mean values of ~320 mm (Hoffman, 1975; Prohaska, 1976). Seasonal mean values are almost constant with ~30 mm/month in summer-autumn and ~20 mm/month in winter-spring (Hoffman, 1975; Prohaska, 1976). During late autumn and winter precipitation falls mostly as snow. The hydrological balance (period 1974–2010) shows an apparent moisture deficit during most of the year, concentrated during November and April, due to high potential evapotranspiration rates (326 mm yr^{-1} in Río Grande; Holdridge, 1978) related to enhanced solar radiation and higher mean monthly temperatures (Tuhkanen, 1992; Villarreal and Coronato, 2017). LLW tend to be more intense in summer and weaker in winter due to the annual cycle of hemispheric pressure.

Berman et al. (2012) and Garreaud et al. (2009, 2013) show that the intensity of regional LLW has a negative correlation with precipitation over the Patagonian steppe. Besides, Berman et al. (2012) document that the passage of low-level synoptic migratory systems is accompanied by significant changes in local weather (i.e., temperature, humidity, precipitation, snowfall, and wind direction). As such, although mean Patagonian winds have a strong westerly component in response to the almost zonal pattern of pressure at high latitudes, the passage of migratory low-level synoptic systems produces significant daily perturbations on the structure of atmospheric circulation.

3. Material and methods

3.1. Coring and sampling

Two sediment cores (LCTF1 and LCTF2) were sampled from Laguna Carmen with a Livingston piston corer and shipped to Instituto de Estudios Andinos (IDEAN), where they were opened, split, described, and sampled. One-half of core LCTF1 (115 cm) was volumetrically sampled at continuous 2.5 cm intervals. Subsamples were split into aliquots for performing biological (ostracod and diatom) analyses and physical (magnetic susceptibility) measurements. The other half of the core was sampled into consecutive 3.75 cm intervals for geochemical analyses. Core LCTF 2 was subsampled for additional and complementary studies and were published elsewhere (*cf*. Coronato et al., 2017; Gogorza et al., 2018; Borromei et al., 2018).

3.2. Core correlation and chronology

A composite age-depth model was developed for LCTF1 based on five ^{14}C datings performed on bulk organic matter from cores LCTF1 and LCTF2 (Supplementary Material, Table 1). Stratigraphic correlation was made using two independent criteria: stratigraphic distribution of ostracods, and sediment features as described by Coronato et al. (2017). Stratigraphic distribution of ostracods for core LCTF2 was published by Borromei et al. (2018). As *Limnocythere rionegroensis* is the most abundant ostracod species, its stratigraphic distribution is used to perform wiggle matching between cores. The most prominent relative abundance variations concerning adjacent samples were chosen as tie points (n=7), while a marked peak in the relative abundance of *Argentocypris sara* (=*Eucypris fontana*) was used as an additional tie point. Linear bivariate regression was performed on these depths to obtain a linear equation linking the depth scales of both cores. A similar procedure was performed with the tie points based on prominent sediment features: the sediment color change at the top of both cores and the presence of distinctive sandy layers in the uppermost part of the cores. The slopes of resulting regression lines were compared employing an F-test (α=0.05) and the overlap of their respective bootstrapped 95% confidence intervals (95% CI, 1999 replicates). All these statistical analyses were performed with the software PAST 3.11 (Hammer et al., 2001). A biostratigraphy-based linear equation relating the depth scales of both cores was used to extrapolate the dated depths from core LCTF2 to core LCTF1. Then, a Bayesian accumulation model (Blaauw and Christen, 2011) was applied to core LCTF1. The model assumes no erosional gaps. AMS radiocarbon ages were calibrated using the SHCal13 curve (Hogg et al., 2013). No local reservoir offset was considered *a priori*. The sedimentation rate was determined iteratively by linear interpolation. Analyses were performed using the Bacon package for R

(Blaauw and Christen, 2011). Beyond the oldest and youngest dating points ages were linearly extrapolated. All modeled radiocarbon ages were rounded to decadal values.

3.3. Sedimentological description, mineralogy, magnetic susceptibility, and geochemistry

Lithofacies were defined according to Miall (1996) considering thickness, color, sedimentary structures, degree of consolidation, grain size, and composition. Grain size was visually determined. The color determination was made using the Rock-Color Chart Committee chromatic standards (Goddard et al., 1951). Representative samples were collected to perform mineralogical studies under a petrographic microscope, regarding textural and compositional parameters. For identification of clay minerals, samples were repeatedly washed in distilled water until deflocculation using Calgon if necessary; the more indurated samples were softly ground with a rubber mortar. The <2 µm fraction was separated by gravity settling from suspension, and oriented mounts were prepared by pipetting a suspension onto glass slides and allowing them to dry. Clay mineralogy was determined from X-ray diffraction (XRD) patterns using samples that were sequentially subjected to air drying, ethylene glycol solvation at 60°C and heating to 550°C for two hours. Diffractograms were run on a Philips X'pert diffractometer, using graphite monochromated Cu radiation at the Instituto de Geociencias Básicas, Aplicadas y Ambientales de Buenos Aires (IGEBA). Semi-quantification of clay mineral contents was performed using peak areas and applying correction factors as proposed by Biscaye (1965).

Low (LF, 470 Hz) and high (HF, 4700 Hz) frequency mass specific magnetic susceptibility (κ) were measured using a Bartington MS2 meter at IGEBA. Major and trace elements (Na, Al, Si, S, K, Ca, Mg, Fe, and Ti) were measured by energy dispersive X-ray fluorescence, using a Shimadzu 720 spectrometer. Spectrometer calibration was carried out by using AGV-2, BCR-2, COQ-1, GSP-2, SGR-1b, and SBC-1 USGS reference materials. Variations of typical detrital elements Si, Al, Ti and Fe, as well as their associations assessed through linear correlation, are interpreted as variations in detrital input allowing inferences on hinterland humid/arid conditions (Davies et al., 2015).

The provenance of terrigenous sediments was estimated based on the Al_2O_3/TiO_2 ratio after Girty et al. (1996). The SiO_2/Al_2O_3 ratio was used to discriminate the detrital input source. Weathering was estimated using a bivariant plot of SiO_2 against (Al_2O_3 + K_2O + Na_2O) (Suttner and Dutta, 1986). The major element composition (TiO_2, Al_2O_3, Fe_2O_3, MgO, CaO, Na_2O, and K_20) was analyzed by discriminant function analysis to determine their settings of provenance (Roser and Korsch, 1988).

Calcium carbonate was determined by calcimetry using a Scheibler calcimeter, and interpreted as the total inorganic carbon (TIC). Total carbon (TC) and total sulfur (TS) were calculated by inductively-coupled plasma optical emission spectrometry (ICP-OES) at the Instituto Nacional de Geología Isotópica (INGEIS). Total organic carbon (TOC) was calculated as the difference between TC and TIC. TOC was interpreted as a qualitative proxy of productivity (Dean and Arthur, 1989; Lyons and Berner, 1992).

3.4. Bioproxies and salinity reconstruction

Sediment samples for ostracod analysis were washed through a 75-µm sieve and dried in a thermostatic oven at 40°C. The dried residue was examined under a stereomicroscope and ostracods were picked. Adults and last instars (A-1) were counted and determined at a specific level based on relevant literature (Cusminsky and Whatley, 1996; Cusminsky et al., 2005; Díaz and Martens, 2014, Pérez et al., 2019). Electrical conductivity (EC), a salinity proxy, was reconstructed through the application of an ostracod-based calibration function developed for Southern Patagonia (Ramón Mercau and Laprida, 2016). The calibration function (r^2=0.74; maximum bias= 0.481 and RMSEP= 0.248) was applied only on samples containing ≥ 50 individuals (absolute abundance). Following the taxonomic analysis of Pérez et al. (2019), the species described as *Eucypris cecryphalium* in Ramón Mercau and Laprida (2016) is ascribed to *Cypridopsis silvestrii*.

Samples for diatom analysis were first treated with 10 % HCl, rinsed, and then heated with 30 % H_2O_2 at 80-90 °C for 2-3 hours. Samples were repeatedly rinsed by suspending and dispersing the material in distilled water. The supernatant was discarded after 2 hours. Permanent slides were mounted with Naphrax® and observed with a light microscope at 1000-x magnification. Diatom identification was based on Krammer and Lange-Bertalot (1986, 1988, 1991a, b) and Rumrich et al. (2000).

4. Results

4.1. Age-depth model

The ostracod-based tie points (Fig. 2A) present an excellent fit to a linear model (r^2=0.98), as well as the sedimentology-based tie points (r^2=0.99) (Fig. 2B). No statistically significant differences were found for the slope values of the regression lines at a 95% confidence level (F=1.96; p=0.21).

Accordingly, the bootstrapped 95% CI of the slopes for the ostracod-based (aO) and sediment-based (aS) correlations were overlapped, with aO CI: 0.89 - 1.12 and aS CI: 0.86 - 0.89.

The resulting age model for LCTF1 (Fig. 2C) estimates an extrapolated mean modeled age of ~4000 cal. BP at 115 cm depth. The youngest well-constrained age estimation is 1150 cal. BP at 8.5 cm. Linear extrapolation of the age-depth model implies a core top age of ~900 cal. BP and coincides with the composite age-depth model proposed by Gogorza et al. (2018) constructed by linear interpolation. The good agreement of paleomagnetic secular variation data (inclination and declination) from Laguna Carmen with those of Laguna Potrok Aike and Lago Escondido allows to discard reservoir effects and confirms a core top age of ~900 cal. BP (Gogorza et al., 2018).

According to the age-model, average sedimentation rates vary from 0.26 mm yr^{-1} between ~4000-2000 cal. BP, followed by a comparatively higher value of 0.61 mm yr^{-1} between 2000-1400 cal. BP, and a lower value of 0.36 mm yr^{-1} for the interval 1400-900 cal. BP (Figs. 2 C).

4.2. Sedimentary lithofacies

The sediment sequence (Fig. 3) comprises heterolithic sandy-silty-clayey sediments (lithofacies Fl and subordinated lithofacies Sr and Fms) dominant from the base up to 65 cm depth, while the upper part of the core consists of clay (lithofacies Fms) with a few interspersed laminae of coarser granulometry (lithofacies Fl).

Lithofacies Fl is composed of thin to thick laminae (1 to 30 mm) resulting from the alternation of fine to medium sand, silt, and clay (Figs. 4 A and B), with wavy lamination. At the base, some load structures of sand overlaying mud layers are preserved. The sand and coarse silt laminae are olive gray (5Y4/1) in colour, and present ripple lamination. The dark greenish gray (5GY 4/1) mud layers almost completely fill the ripple troughs and form a thin cover over the crests, following approximately the undulating shape of the underlying structures. In some cases, the clay layers are discontinuous and do not reach the crests of sand layers. The wavy bedding of the sand layers is vertically discontinuous. Sand layers occasionally present normal grading.

Lithofacies Fsm (Fig. 4C), which can be distinguished from lithofacies Fl by the lack of sand beds (Miall, 1996), constitutes of layers with thin to medium bedding, composed by olive grey (5Y 4/1) or light olive grey (5Y 5/2), massive fine silt and mud. Drying shrinkage cracks in some banks due to contraction of expanding clays after core opening are observed (Fig. 4D). Occasionally, vertically and laterally discontinuous fine sand lenses occur (Fig. 4E). These incomplete small sand ripples are formed in a muddy substratum and are preserved because of deposition of a new mud layer, thus giving rise to lenticular bedding (Fig. 4F). The sand supply is poor so that only a few incomplete ripples are produced (Reineck and Singh, 2012; Boggs, 2014).

Lithofacies Sr comprises grayish orange pink (5Y 8/1) fine to medium sand and coarse silt, with small-scale crossbedding. Individual units are few mm up to 1 cm thick and can have graded bedding (Fig. 4G). Cross-bedding results from migration of small ripples during periods of current activity. Small flasers are shown in Fig. 4H.

4.3. Petrographic composition and mineralogy

The petrographic composition of sand and coarse silt fractions is dominated by volcanic lithoclasts, with an average quartz-feldspar-rock fragment ratio of 10:38:52. All the samples share the same heavy mineral assemblage: augite, hypersthene, hornblende, opaques, and vestiges of biotite. The associations of heavy and light minerals indicate provenance from the magmatic arc of the Andes.

The mineral composition of pelitic samples inferred by XRD analysis is homogeneous across the sequence. Plagioclase is the dominant component (>50%), accompanied by abundant quartz, variable amounts of (magnesian) calcite, clay minerals and, in some cases, minor quantities of zeolite and cristobalite (Supplementary Material, Figure 1). XRD analyses of a <2 µm fraction of lithofacies Fsm revealed that clay minerals consist mainly of fine-grained mafic phyllosilicate, almost exclusively smectite, with a scarce contribution of poorly crystalline illite/smectite and traces of illite and chlorite. Glass shards are dispersed through most of the core. A predominantly detrital origin is suggested for the clay minerals.

The discriminant function diagram for the provenance signature of sediments (Supplementary Material, Fig. 2A) shows that most samples plot within (or very close to the limit of) the field of mature polycyclic continental sediments (Roser and Korsch, 1988). The bivariate SiO_2 vs. (Al_2O_3 + K_2O + Na_2O) plot (Supplementary Material, Fig. 2B) points to prevalence of semi-arid conditions during weathering and transport of these sediments (Suttner and Dutta, 1986).

4.4. Magnetic susceptibility and geochemistry

63% of samples represent Al_2O_3/TiO_2 ratios lower than 14 (Fig. 5) and point to predominance of mafic rocks as the source of detrital input (Girty et al., 1996). This agrees with petrographic observations of abundant mafic minerals in the sandy fraction as well as the positive correlation between Ca and Fe (r^2= 0.58, p< 0.05) and Ca and Mg (r^2= 0.84, p> 0.05). Prominent peaks of the Al_2O_3/TiO_2 ratio (>15) allow inferring intermediate to acid igneous input at 1180, 1890, and between 3250-3490 cal. BP (Fig. 5). These samples are in or close to the field of andesitic rocks in the discriminant diagram (Supplementary Material, Fig. 2A). Together with the presence of glass shards, conspicuous peaks of Si, Al, and Na, and the decrease in Ti, Ca, Fe, Mg and the Si/Al ratio between 1120-1230, 1820-1890 and 3250-3490 cal. BP (Fig. 5), suggest the presence of reworked acid volcanic ashes, not distinguishable by visual examination as tephra layers. Values of Al_2O_3/TiO_2 indicate mixing of ash with non-volcanic material, probably detrital quartz (Senkayi et al., 1984). Oscillations of the mass specific magnetic susceptibility (κ) (Fig. 5) throughout the core range between 0.06 and 19.3 $10^{-7}m^3kg^{-1}$. Changes of κare associated with variations in overall particle size, with highest values coinciding with lithofacies Sr and Fl and those levels with inferred higher contributions of volcanic ash particles.

Overall, geochemistry varies moderately throughout the core (Fig. 5). Variations in major element concentration are more significant in the upper half of the core, characterized by fine-grained lithology. In agreement with XRD results, Ca and Mg as well as Si and Al vary jointly in lithofacies Fsm (r^2=0.97; p<0.05 and r^2=0.85, p< 0.05, respectively). Fe and Ti present a positive correlation (r^2=0.75; p<0.05), showing higher concentrations in lithofacies Fl and Sr. For their part, Fe and Al concentrations show a strong negative correlation (r^2= -0.86, p<0.05). This behavior may be due to the presence of Fe-bearing mafic minerals in those lithofacies, while higher contents of Al are mostly related to clay-rich lithofacies Fsm. TC and TOC (Fig. 6) document low variability and relatively low average values (2.29 and 1.12 wt %, respectively). Lower values of TOC tend to coincide with the occurrence of lithofacies Fl and Sr in the lower half of the sequence, whereas peaks (~3 wt%) occur mainly in lithofacies Fsm. TIC oscillates between 0.46 and 1.93 wt%, with an average value of 1.17 wt%; there is no correlation between TOC and TIC (r^2=-0.21, p=0.16). Based on petrographic analyses and considering that TIC peaks tend to occur in lithofacies Fl and Sr, we suggest that variations in TIC reflect variations in detrital input rather than lake level fluctuations or changes in biogenic accumulation. TS does not correlate with TOC (r^2=0.23, p=0.21), but correlates strongly with Ca (r^2= 0.59; p= 0.007) suggesting that TS can be used as a proxy of salinity (Cohen, 2003).

4.5. Bioproxies and electrical conductivity reconstruction

Ostracod valves were recovered from almost all samples analyzed. Absolute abundances range between 3 and 407 valves per gram (Fig. 7). Only five samples were devoid of ostracods, while 15 samples present low absolute abundances and are deemed sterile for quantitative environmental reconstruction. Seven species were identified, with each assemblage comprising one to six species (median species richness S = 3); *Limnocythere rionegroensis* and *Cypridopsis silvestrii* were codominant, contributing 41% and 39% of individuals in the total fossil assemblage, respectively. The remaining species present are *Newnhamia patagonica*, *Argentocypris sara* (= *E. fontana*), *A. virgata*, *A. sarsi*, and *L. patagonica*.

The EC calibration function was applied to the compositional data of samples with > 50 individuals of absolute abundance, allowing EC reconstruction between 1350-3590 cal. BP (Fig. 7). The reconstruction yielded EC values ranging from 1220 ± 90 to 9100 ± 600 µS/cm (average: 3900 ± 300 µS/cm), corresponding to salinity values within the oligo- and lower mesohaline ranges. Shifts in reconstructed EC coincide with lithofacial changes: samples corresponding to lithofacies Fl and Sr usually yield relatively low EC values, while most samples corresponding to lithofacies Fsm yield relatively high EC values.

44% of samples are devoid of diatoms, and no valves were found before 2700 cal. BP (Fig. 8). The number of diatoms was strikingly low; almost half of them present only fragmented valves. Twenty-seven species were recognized, fifteen of which were left in open nomenclature due to poor preservation. Diatoms are more abundant in lithofacies Fsm and tend to diminish between 1120-1230 and 1840—1900 cal. BP, in coincidence with levels interpreted as reworked volcanic ashes. *Diploneis* sp. and S*urirella tuberosa* O. Müller make up 45% and 32% of the total assemblage, respectively (Fig. 8). In the topmost levels, *Craticula halophila* (Grunow) D.G. Mann and *Diploneis elliptica* (Kützing) Cleve are relatively abundant. Several taxa (*Achnanthe*s sp., *Aulacoseira* sp., *Denticula* sp., *Encyonema* sp., *Eunotia* sp., *Eunotia arcus* Ehrenberg, *E. tecta* Krasse, *Fragilaria virescens* Ralfs, *Gomphonema parvulum* (Kützing) Kützing, *Hantzchia* sp., *Navicula capitata* Ehrenberg and *Stauroneis* sp.) are found in at most two samples and in very low abundances.

5. Discussion

The Bayesian age-depth model indicates that the core LCTF1 spans the period between ~4000-900 cal. BP. No erosional gaps have been identified based on sedimentology or magnetic parameters (Gogorza et al., 2018). Our age-depth model coincides with the composite age-depth model proposed by Gogorza et al. (2018) based on linear interpolation of datings and tuned by paleomagnetic secular variation (PSV), but differs from the model proposed by Borromei et al. (2018) for core LCTF2, based on linear interpolation assuming a core-top age of 0 cal. BP. A core-top age of ca. 900 cal. BP reflects the modern erosive force of LWW and the deflation processes that affect the lake basin during driest summers, as evidenced by large dune field migrating eastward from the lakeshore (Coronato et al., 2017; Villarreal and Coronato, 2017).

According to the age-depth model, the average sedimentation rate for the composite profile is 0.3 mm $yr^{-1}$and increases from 0.26 mm yr^{-1} to 0.61 mm yr^{-1} at ~2000 cal. BP.

5.1. Identification of sediment sources

Lacustrine sediments (mostly smectite and mafic volcanic lithoclasts, Supplementary Material, Figs. 1 and 2A) have been formed by physical weathering of Castillo and Carmen Silva Formations, however the presence of volcanic glass shards indicates frequent contributions of fine-grained volcanic material from the Austral Volcanic Zone (AVZ, 49-55 °S). Ordination analysis identifies 3 samples placed within (or very close to) the field of dominantly andesitic composition and hence, within the geochemical signature of volcanic rocks from the AVZ (Supplementary Material, Fig. 2B). Thus, they can be interpreted as lacustrine sediments *enriched* in volcanic ash. Centered at ~3290 cal. BP, ~1890 cal. BP, and 1180 cal. BP, they they would be linked with some Late Holocene explosive eruptions of the AVZ: the A1 event of the Volcán Aguilera (53°S-70°W, 2546 masl) at 3120 ± 140 cal. BP; the R2 event of the Volcán Reclus (50°57'50"5-73°35'W, 1000 masl) at 1880 ± 30 cal. BP; and the R3 event of the same volcano, considered as being older than 940 ± 40 cal. BP but younger than 1050 ± 60 cal. BP (Moy et al., 2008; Fontijn et al., 2014). Although a better geochemical characterization is needed to corroborate this link, their chronology provides additional support for our age-depth model and confirm the role of AVZ volcanoes as fine-grained sediment sources for the shallow lakes of the Fuegian steppe.

5.2. Paleoenvironmental reconstruction

The lithofacies association is interpreted as deposition in a shallow lake under alternating wet and dry conditions. Wet intervals with recurring bottom current activity were more frequent between

4000-2200 cal. BP, when lithofacies Sr and Fl predominate (Fig. 3), probably associated with streams responsible for the transportation of sand and coarse silt after rains and/or the melting of snow during spring. In lithofacies Sr, cross-bedding results from migration of small ripples during periods of current activity. Flaser structure is formed when the currents cease, and the mud falls out of suspension and deposits on top of the ripples. When starting a new cycle, ripple crests are eroded and sand is deposited as ripples, covering and preserving the cross-bedding with flasers in the troughs. This implies that conditions for deposition and preservation of sands were more favorable than for mud (Reineck and Singh, 2012; Boggs, 2014). In lithofacies Fl, the wavy bedding needs specific conditions, where the sedimentation and preservation of sand and mud layers are possible (Reineck and Singh, 2012; Boggs, 2014). This sedimentary structure is consistent with alternating deposition conditions. When weak tractive currents are active, sand and coarse silt are transported and deposited as ripples. When the currents cease, mud in suspension falls, and completely cover the ripples. Load structures preserved at the base of the sand overlaying mud layers were the result of deposition of sand over a hydroplastic mud layer. Drier periods with no current activity were more frequent since 2200 cal. BP and especially since 1600 cal. BP. The predominance of lithofacies Fsm since 2200 cal. BP (Fig. 3) suggests deposition in a shallow lake deprived of fluvial inflow under conditions of limited rainfall. The eolian transport could have played an important role for the influx of fine-grained particles. The presence of eolian landforms such as mantles, plumes and perched dunes in Laguna Carmen and other shallow lakes of the region (Coronato et al., 2017, 2020), confirm that wind is an important geomorphological agent for sediment transport in the northern Fuegian steppe. The occasional presence of lithofacies Fl since 2200 cal. BP would represent periods of higher humidity and weaker current activity. Thereafter, climatic-driven aridification increased at some time after 1000 cal. BP, and the modern dynamic of the lake was established. The result was a decrease in lake level and the beginning of frequent dessiccation events during dry summers, leaving the lake sediments exposed to deflation. The age-depth model shows that these dessication events would have started less than 1000 years ago.

Reconstructed EC values reflect the onset of drier conditions around ~2200 cal. BP (Fig. 7). Between 3550-2250 cal. BP, when lithofacies Sr and Fl predominate, EC mainly yields values in the lower oligohaline range (mean: 2554 µS/cm), and tends to increase to an upper oligohaline-mesohaline range (mean: 4799 µS/cm) since 2250 cal. BP, when massive fine silt and mud (lithofacies Fsm) constitute the sediment sequence.

It is only after around 2300 cal. BP that diatom taxa become present in core LCTF1 (Fig. 8). Assemblages are dominated by robust benthic taxa. Small taxa are rare, fragmented, or partly dissolved. This suggests one or more strong taphonomic filters acting on these diatom assemblages. Differential breakage and/or dissolution of species bias the composition of assemblages towards more robust taxa (Battarbee et al., 2005). Diatom frustule preservation in lacustrine sediments is affected by several factors acting during sedimentation and burial: high pH and salinity, carbonate precipitation, high frequency or duration of lake mixing, turbulence, and high-temperature favor silica dissolution and valve breakage, while increased water depth and high sedimentation rates promote valve preservation (Ryves et al., 2006). High degree of diatom valve dissolution and breakage has been observed in samples from the top of several records in Patagonia, corresponding to amazingly low values of diatom concentration (Recasens et al., 2012). Most of the Holocene diatom assemblages show strong signs of dissolution since the onset of more saline conditions (i.e., Massaferro and Larocque-Tobler, 2013; Recasens et al., 2015). At Laguna Carmen, reconstructed EC values are within the meso-oligohaline range for most of the record, which suggests that the absence or poor diatom preservation could not be assigned to high salinity or carbonate precipitation but to the predominance of physical conditions favoring diatom breakage. The shallow water depth of the lake and its geographic location in the windy and cold northern Fuegian steppe would account for wave turbulence under partly subaerial conditions and frequent resuspension cycles which could have caused the mechanic destruction of diatom valves, making them more liable to dissolution (Bennion et al., 2010) and favoring the preservation of larger-celled, heavy diatoms during intense periods of mixing (Huisman et al., 2002). However, the absence of diatom valves or fragments before 2300 cal. BP could also be attributed to other limnological variables such as thick and persistent ice cover, limited light, nutrients and habitat availability (Perren et al., 2003), since ostracods, which would be much more prone to physical breakage, are relatively well preserved in the same levels where diatoms are absent.

The geochemical profiles (Fig. 5) show patterns that could be related to variations in surface runoff and salinity. Relative higher values of Fe and Ti between 4000-2000 cal. BP (Fig. 5) allow inferring higher input via runoff primarily of weathering products from surrounding mafic rocks. Moreover, TIC values (Fig. 6) show a similar pattern, with higher values coinceding with coarser grain sizes suggesting enhanced detrital calcite input derived from the calcite-bearing fossiliferous conglomerates of the Carmen Silva Formation during deposition of lithofacies Sr and Fl. As such, higher (lower) concentration of Fe, Ti and TIC would reflect higher (lower) detrital input to the lake and, coincident with lower (higher) reconstructed EC values, indicate a relative higher (lower) lake level. In turn, EC and TS correlate (r^2=0,54; p<0.01), confirming that TS increases with salinity. The gradual shift in geochemical parameters, the increase in EC and the predominance of lithofacies Fsm since 2200 cal. BP would imply a limitation of water and sediment input from inflows due to lower precipitation and changes in hydological balance.

Shallow lakes are productive systems: productivity is a consequence of nutrients, which are more readily available from the lake bottom as well as more extensive littoral habitats for primary producers (Dodds and Whiles, 2020). The presence of colonies of green algae such as *Pediastrum* and *Botryococcus braunii* and pollen from aquatic vascular plants (Borromei et al., 2018), diatoms, and ostracods in the Laguna Carmen sedimentary record allow inferring that lake productivity was high enough to sustain a complex ecosystem. Even if allochthonous input of organic matter from the catchment area cannot be ruled out, soils in the Fueggian steppe show incipient degrees of accumulation of organic matter and low edaphic development (Pereyra and Bouza, 2019). Although Late Holocene paleosols have been described, they were rapidly buried by eolian and colluvial deposits (Favier-Dubois, 2007; Coronato et al., 2020). Additionally, Borromei et al. (2018) considered that an increase in the amorphous organic matter content in LCTF2 was produced by bacterial action on *Botryococcus braunii* and *Pediastrum* under oxygen deficiency. Therefore, our understanding is that the primary source of organic matter of LCTF1 is particulate detritus of plants and algae that lived in the lake waters and the littoral habitats. We consider that TOC can be used as a reliable proxy of lake productivity. Preservation of organic matter could have been favored by lake water isolation by ice cover during winters. Ice cover not only impedes oxygen diffusion across the air water-interface but also wind-induced mixing favoring water stagnation and reduces primary production, which constitutes another supply of oxygen for respiration and abiotic oxidation (Pulkkanen and Salonen, 2013). As such, low values of TOC (Fig. 6) indicate that Laguna Carmen was a lake of low productivity between ca. 4000-2700 cal. BP, the lowermost values in coincidence with lithofacies Fl-Sr. Low ostracod abundance reinforces this hypothesis. On the other hand, relative high values of TOC after 2700 cal. BP reflect a slight increase in productivity, interrupted by a pulse of low productivity centered at 1650 cal. BP, in coincidence with lithofacies Fl, a lowering in the absolute abundance of ostracods and the absence of diatoms. Peaks in lake productivity appear to have occurred at 3750, 2000, 1750 and 1470 cal. BP and coincide with lithofacies Fsm.

In summary, the combination of sedimentological, biological, and geochemical proxies of LCTF1 allow to reconstruct centennial-scale variations in salinity, productivity, water regime, and sedimentary input driven mainly by changes in water balance induced variations of the lake level. Between 4000 and 2200 cal. BP, EC values and lithofacies correspond to a predominantly wet period and a high lake level is maintained by active discharge of the lake's tributaries due to the (overall) positive hydrological balance. During this period, lacustrine productivity was relatively low but increased gradually since 2700 cal. BP. Since *ca*. 2200 cal. BP, higher EC values and massive pelitic deposits mark the onset of a period of negative hydrological balance, a reduction of the transport capacity of tributaries and lower lake levels. Higher absolute abundance of ostracods, preservation of diatom assemblages since 2300 cal. BP and higher values of TOC since 2100 cal. BP, indicate that Laguna Carmen gradually became a moderately productive lake. The age of the top of the core is evidence that the climate became drier and the shallow lake was replaced by the modern pan sometimes after 1000 cal. BP.

5.3. Paleoclimatic reconstruction and Holocene climate drivers in Southern Patagonia

During the Holocene, prior to any anthropogenic forcing, the main driver of long-term climate change was the shift in seasonal and latitudinal distribution of incoming solar radiation (insolation) due to changes in orbital parameters of the Earth (Wanner et al., 2008). In the Southern Hemisphere, insolation throughout the Holocene increased in summer-autumn and decreased in winter-spring (Berger, 1978). Paleoclimatic simulations performed with state-of-the-art numerical models describe significant changes in meridional pressure gradients for the entire troposphere as a consequence of these insolation changes that, in turn, induce significant changes in intensity of the LLW (Rojas and Moreno, 2011). Model simulations describe increasing Westerlies over southern Patagonia from late summer to winter and significant reduction of wind intensity during spring. Regarding temperature changes through the Holocene, model simulations describe progressive warming over Patagonia from 6000 cal. BP to pre-Industrial times in austral summer-autumn-winter and a cooling during spring (Berman et al., 2017).

As most lakes in semi-arid regions (Lamb et al., 1999), the paleoenvironmental evolution of Laguna Carmen seems to have been dominated by changes in water balance. Long-term trends on water level and conductivity between ~4000-1000 cal. BP indicate a marked change in water balance of the lake from wetter to drier conditions throughout the Late Holocene. The lake finally became a pan exposed to deflation processes sometimes after 1000 cal. BP. This scenario of increasing water deficit is consistent with the strenghtening of the LWW and concomitant decreasing precipitation from January to July, as well as with progressive warming especially during austral summer-autumn since 6000 cal. BP as indicated by climate model output (Rojas and Moreno, 2011; Berman et al., 2017).

Between ~4000-2200 cal. BP, colder temperatures during autumn and winter, and milder temperatures during spring (Berman et al., 2017) favored winter snow accumulation and streams with larger amounts of sand and coarse silt carried to the lake during the milder-than-present springs. As the intensity of regional LLW has a negative correlation with precipitation over the Patagonian steppe, weaker LLW in austral summer-autumn implies higher precipitation. The consequent increase in stream and overland water flow caused higher water levels, oligohaline salinities, and a higher total content of Fe and Ti. Lower salinities, higher lake levels, and colder air temperatures could have promoted prolonged ice cover during early Late Holocene winter seasons The absence of diatom valves before 2300 cal. BP indicates that assemblages have been dominated by taxa prone to dissolution or even absence of living diatoms during the time of sediment deposition as a consequence of thicker and persistent ice cover and limited light (Perren et al., 2003, Paull et al., 2017). Thereafter, a diatom community shift occurred, and taphonomic processes (mainly high turbulence and holomixis during warm and windy springs) favored preservation of larger-celled benthic diatoms.

A climatic threshold seems to have been reached about 2200 cal. BP. The progressive warming together with stronger LLW during late summer-autumn-winter due to changes in seasonal and latitudinal distribution of insolation (Rojas and Moreno, 2011; Berman et al., 2017) have affected water balance negatively. Lithofacial analysis indicates that evidences of tractive currents diminished, indicating a marked decrease in precipitation. The decrease in stream and overland water flows and the increased wind-induced evaporation have caused a lowering of the lake level, and together with evaporative concentration related with higher summer temperatures, caused higher salinities and enhanced lake productivity.

Lithofacies, EC reconstruction and selected geochemical parameters (TIC, TS) indicate that this long-term tendency towards drier conditions was punctuated by short-term variability in water balance. The colder and wetter period between 4000-2200 cal. BP was interrupted by predominantly drier conditions lasting several decades, centered at 3750, 3150 and 2700 cal. BP. Multiple factors could produce drier decades in Southern Patagonia. Considering characteristics of present-day climate, changes in interaction between the El Niño-Southern Oscillation (ENSO) and the Southern Annular Mode (SAM, Berman et al., 2012, 2013) and feedbacks between ENSO and the Antarctic Circumpolar Wave (White et al., 2002) are examples of coupled atmosphere-ocean processes affecting low-frequency variability of Patagonian climate. These large-scale atmospheric patterns might induce less frequent and/or less intense migratory cyclones and frontal systems to pass the middle and high latitudes rather than a strengthening of the LLW.

Conversely, the dry and milder period between 2200-1000 cal. BP, was interrupted by relative short wetter periods centered at 2030 and between 1700-1600 cal. BP, probably associated with more frequent and/or more intense migratory cyclones and frontal systems. At some time after 1000 cal. BP, modern semi-arid conditions began to prevail due to long-term insolation trends, which imply stronger LLW and higher temperatures during summer-autumn-winter (Rojas and Moreno, 2011; Berman et al., 2017). Although it is not possible with the presented data to determine the timing when current conditions started and the lake began to dry out, the aeolian landforms identified by geomorphological analysis of the lake basin (Coronato et al., 2017) indicate that these conditions were established several centuries ago.

5.4. Comparison with other records from Southern Patagonia

The comparison of timing and nature of paleoclimate changes reconstructed for Laguna Carmen with other paleoenvironmental records between 49º-53ºS is complex. Southern Patagonia is a region with strong topographic and climatic gradients. Processes studied at small spatial scales in western Tierra del Fuego at 53°S (Schneider et al., 2003) show that although temperatures are generally similar, differences in local cloud cover are determined. Overall, wind speeds are not only higher in the mountains, but also at easternmost sites. Likewise, the distribution of precipitation is susceptible to small-scale inhomogeneities in local topography and the local manifestation of climate (i.e., wind exposure and speed or lake ice phenology such as presence/absence, freeze-up/break-up and duration of ice cover).

To place our paleoclimate interpretation into a regional context, we compare it with other records from Southern Patagonia including the paleoenvironmental reconstruction of Laguna Carmen proposed by Borromei et al. (2018), although differences of age-depth models make comparison disputable. Thus, comparison is limited to the core section where this age model is constraint by the uppermost dated level (1380 cal. BP). Within geochronological uncertainties, our conductivity and lake level reconstructions partially coincide with those proposed by Borromei et al. (2018). Wetter conditions between 3600-3300, 2100-2000 and around 1600 cal. BP, and drier conditions between 3800-3700, 1900-1700 and since 1400 cal. BP have been proposed for both reconstructions, although the temporal extension of these events is different. Conversely, tendencies of opposite sign in water balance were reconstructed between 3000-2800 cal. BP and 2600-2100 cal. BP. Intervals that Borromei et al. (2018) defined as predominantely dry we consider as wetter. Despite these similarities and contrasts, there are differences in EC values: while EC values reconstructed by Borromei et al. (2018) reflect meso-oligohaline salinities, our results reflect mostly oligohaline conditions. This difference can be attributed to differences in statistical theory and methodology applied, especially the calibration set used and the model chosen for calibration (Birks and Birks, 2006; Bjune et al. 2010; ter Braak and Juggins 1993; Birks et al., 2010, 1998; ter Braak, 1986; ter Braak and Looman 1995).

Studies on perched dunes on the Fuegian steppe located at the periphery of shallow lakes Arturo, Amalia and O´Connor (53°S) have pointed to alternating semi-arid (eolian deposits) and wet (paleosols) periods during the Holocene (Orgeira et al., 2012; Coronato et al., 2011, 2020). Although the chronology of these paleosols is problematic, paleosols Ps 5 and Ps 6 from the Amalia dune, and Ps 7 and Ps 8 from the Arturo dune (Coronato et al., 2020) fit with the wetter period between 4000-2200 cal. BP we defined for Laguna Carmen. In turn, paleosol Ps 7 of the Amalia dune could be correlated with the wetter event centered at 2030 cal. BP. Noticeably, no paleosols were recognized within the dry period as defined by LCTF1 between 1500 - 900 cal. BP.

Paleolimnological records from the continental Southeastern Patagonia steppe provide a consistent regional picture concerning the hydrological balance since 4000 cal. BP (Figs. 9 and 10). At Laguna Potrok Aike, the abundance of Andean Forest Taxa (AFT) does not show a clear long-term trend, but slightly lower values between 4000 and 2350 cal. BP (Wille et al., 2007) have been interpreted as moister conditions (Fig. 9B). According to Mayr et al. (2007), the relative high values of AFT flux between 2300-1400 cal. BP (Fig. 9C) would indicate drier conditions, in coincidence with our interpretation for Laguna Carmen. Chironomid-based mean annual temperature reconstruction (Massaferro and Larocque-Tobler, 2013) shows a drop at 3800 cal. BP leading to estimations of colder than present temperatures between 3500-2000 cal. BP, and at around 1600 cal. BP (Fig. 9D), in coincidence with predominantly wet periods at Laguna Carmen. At Laguna Azul, several centennial warm/dry periods overprinted the multi-millennial Holocene hydroclimatic variability during the last 4000 years (Zolitschka et al., 2018). Diatom assemblages indicate fluctuating lake levels and salinities, whereas the increase in *Nothofagus* around 3000 cal BP documents intense aridity (Fig. 9E). Elevated TIC was interpreted as century-long warm/dry events that occurred at around 2200 (TIC8) and 1300-1000 cal. BP (TIC9). In summary, eastern Patagonian steppe lakes reflect moister and colder conditions during the early Late Holocene, and drier and milder conditions since ~2200 cal. BP, in general agreement with our reconstructions.

Hydrologic balance at high-altitude sites in the South Patagonian steppe compare to those of southwestern Patagonia, where the strong Westerlies are associated with higher precipitation. According to Fey et al. (2009), precipitation associated with easterly airflow cannot reach the high-altitude sites as frequently as the lowland sites in the east. Based on this scheme, Ohlendorf et al. (2014) analyzed the Laguna Cháltel record. A period of lake desiccation at around 4800 cal. BP was followed by a shift towards a positive water balance between 4000 - 3200 cal. BP, and a sustained lake level rise during the Late Holocene (Fig. 10 B). The lake-level increased at around 3200 and 1600 cal. BP and no desiccation events were recognized until present.

The wet and cold period between 4000-2200 cal. BP proposed for the Fuegian steppe coincides with the so-called Late Holocene Warm/Dry Period in western Patagonia (Moreno et al., 2009; Pérez-Rodríguez et al., 2016). Moreno et al. (2014, 2018) analyzed the sedimentary record of Lago Los Cipreses, Torres del Paine National Park (TPNP), Chile. The record indicates that between 4000-2700 cal. BP, the Late Holocene was predominantly warm and dry, peaking at 3850, 3360, and 2900 cal. BP (Fig. 10C). Therafter, predominantly cold/wet conditions prevailed, overprinted by warm/dry episodes at 2300, 1530 and 915 cal BP. The beginning of humid conditions roughly coincides with the dry interval of Laguna Carmen centered at ca 2700 cal. BP. According to Moreno et al. (2018), intervals of reduced precipitation brought by the SAM-like positive events and weak LWW were followed by a multi-millennial rise in precipitation related to SAM-like negative events and stronger LWW since 2700 cal. BP. Afterwards, dry conditions prevail in the eastern lowlands, whereas western Patagonia displayed predominantly cold/wet conditions, especially since 1400 BP. Pollen and charcoal analyses of Lago Guanaco at the TPNP, reflects relatively wet intervals at 2900–1900 and 1300–1100 cal. BP (Fig. 10D) related with increased LWW (Moreno et al., 2009). Pérez-Rodríguez et al. (2016) analyzed the sedimentary record of Lago Hambre at the coast of the Strait of Magellan. Low mineral matter accumulation was interpreted as relatively dry conditions between 4000-3700, 3500-3100, 2900-2550 and 2150-1700 cal. BP enforced by weaker LWW, whereas isolated wet events were detected at 3600, 3090 and 2250 cal. BP (Fig. 10E). Since 1700 cal. BP, wetter conditions prevailed punctuated by multidecadal dry conditions centered at 1450 and 1100 cal. BP. Turney et al. (2016) analyzed charcoal and *Nothofagus* concentrations in an exposed -grass peatland at Canopus Hill, Malvinas (Falkland) Islands. Their results suggest that the LWW were particularly strong between 2000 and 1000 cal. BP with a prominent peak at approximately 1800–1300 and 1000 cal. BP (Fig. 10F). Stronger westerly flow over the Malvinas Islands roughly coincides with the onset of drier conditions at Laguna Carmen.

6. Conclusions

The Late Holocene sedimentary record of the Laguna Carmen, a shallow lake located in the northern Tierra del Fuego steppe, reflects the shift from wetter to drier conditions at around 2200 cal. BP, and the onset of modern semi-arid conditions sometime after 1000 cal. BP, when the LLW became the principal geomorphological agent generating substantial deflation on soils and surficial sediments. Our results are in accordance with paleoclimatic models suggesting that southernmost Patagonia has suffered a progressive warming and a strengthening in LLW intensity during summer and winter of the Late Holocene. This caused changes in lake water balance. The progressive aridification since 4000 cal. BP would reflect the strengthening of LLW, but it might also be associated with increased temperature in response to insolation changes. In fact, changes in Earth's orbital parameters since 4000 yr BP increased insolation over Patagonia in summer and autumn which, in turn, induced regionally warmer conditions during winter.

Southern Patagonia is topographically complex and additionally the local manifestation of climatic conditions obscures the regional climatic trends. Combining studies of deep and shallow lakes, east and west to the Andes with continuous subaqueous sedimentation needs to be encouraged to integrate spatial and temporal large-scale (e.g., regional and millennial) and small-scale (e.g., local and multidecadal) climate reconstructions.

Acknowledgments

This work was supported by the Agencia Nacional de Promoción de Ciencia y Técnica of Argentina (grant PICT 2012-0628), the National Research Council of Argentina (CONICET; grant PIP 11220080101161) and the University of Buenos Aires (grant UBACyT 20020150100026BA). We would like to thank to Dr. Bernd Zolitschka and an anonymous reviewer for taking time and effort necessary to provide insightful guidance and comments on the paper, as these comments improved this work. This is the IDEAN contribution #123.

References

Battarbee, R.W., Monteith, D.J., Juggings, S., Evans, C.D., Jenkings, A., Simpson, G.L., 2005. Reconstructing pre-acidification pH for an acidified Scottish loch: a comparison of palaeolimnological and modeling approaches. Env. Poll. 137, 135-149.

Bennion, H., Sayer, C.D., Tibby, J., Carrick, H.J., 2010. Diatoms as indicators of environmental change in shallow lakes, in: Smol, J.P., Stoermer, E.F. (Eds.), The Diatoms: Applications for the Environmental and Earth Sciences. Cambridge University Press, pp. 152- 173.

Berger, A., 1978. Long-term variations of daily insolation and Quaternary climatic changes. J. Atmos. Sci. 35, 2362–2367.

Berman, A.L., Silvestri, G., Compagnucci, R., 2012. Eastern Patagonia seasonal precipitation: influence of southern hemisphere circulation and links with subtropical South American precipitation. J. Clim. 25, 6781–6795.

Berman, A.L., Silvestri, G., Compagnucci, R., 2013. On the variability of seasonal temperature in southern South America. Clim. Dyn. 40, 1863–1878.

Berman, A.L., Silvestri, G., Rojas, M., Tonello, M., 2017. Accelerated greenhouse gases versus slow insolation forcing induced climate changes in southern South America since the Mid-Holocene. Climate Dynamics 48, 387–404.

Birks, H.H., Birks, H.B.J., 2006. Multi-proxy studies in palaeolimnology. Veget. Hist. Archaeobot. 15, 235-251. doi.org/10.1007/s00334-006-0066-6.

Birks, H., Birks, H.D.G. Frey, Deevey, E.S., 1998. Review 1: Numerical tools in palaeolimnology. Progress, potentialities, and problems. Journal of Paleolimnology 20, 307–332. doi.org/10.1023/A:1008038808690.

Birks, H.J.B., Heiri, O., Seppä, H., Bjune, A.E., 2010. Strengths and weaknesses ofquantitative climate reconstructions based on late-quaternary biologicalproxies. Open Ecol. J. 3, 68–110.

Biscaye, P.E., 1965. Mineralogy and sedimentation of recent deep-sea clay in the Atlantic Ocean and adjacent seas and oceans. Geol. Soc. Am. Bull. 76, 803–832.

Bjune, A.E., Birks, H.J.B., Peglar, S.M., Odland, A., 2010, Developing a modern pollen-climate calibration data-set in Norway. Boreas, 39, 674-88.

Blaauw, M., Christen, J.A., 2011. Flexible paleoclimate age-depth models using an autoregressive gamma process. Bay. Anal. 6, 457–474.

Boggs, S. Jr., 2014. Principles of sedimentology and stratigraphy. Fifth Edition. Prentice Hall.

Borromei, A.M., Candel, M.S., Musotto, L.L., Cusminsky, G., Martínez, M.A., Coviaga, C.A., Ponce, F., Coronato, A., 2018. Late Holocene wet/dry intervals from Fuegian steppe at Laguna Carmen, southern Argentina, based on a multiproxy record. Palaeo. Palaeo. Palaeo., 499, 56-71.

Braconnot P., Harrison, S.P., Kageyama, M., Bartlein, P.J., Masson-Delmotte, V., Abe-Ouchi, A., Otto-Bliesner, B., Zhao, Y., 2012. Evaluation of climate models using palaeoclimatic data. Nat. Clim. Change 2, 417–424. doi.org/10.1038/nclimate1456.

Codignotto, J.O., Malumián, N., 1981. Geología de la región al Norte del paralelo 54º S de la Isla Grande de Tierra del Fuego. Rev. Asoc Geol. Arg. 36, 44-88.

Cohen, A.S., 2003. Paleolimnology: The History and Evolution of Lake Systems. Oxford University Press.

Coronato, A., Fanning, P., Salemme, M., Oría, J., Pickard, J., Ponce, J.F., 2011. Aeolian sequence and the archaeological record in the Fuegian steppe, Argentina. Quat. Int. 245, 122–135.

Coronato, A., Salemme, M., Oría, J., Mari, F., López, R., 2020. Perched dunes in Fuegian steppe, southern Argentina: archeological reservoirs of Holocene information, in: Collantes, M.M., Perucca, L., Niz, A., Rabassa J. (Eds.), Advances in Geomorphology and Quaternary studies in Argentina. Special Symposium from the Argentine Association of Geomorphology and Quaternary Studies. Springer Earth System Sciences, pp. 58-91.

Coronato, A.M.J, Ponce, J.F., Quiroga, D.R.A., Gogorza, C., 2017. Caracterización geológica y geomorfológica de la cuenca de la laguna Carmen (estepa fueguina, Argentina) y su registro sedimentario durante el Holoceno tardío. Rev. Asoc. Geo. Arg. 74, 263-273.

Coviaga, C., Cusminsky, G., Peréz, P., 2017. Ecology of freshwater ostracods from Northern Patagonia and their potential application in paleo-environmental reconstructions. Hydrobiol. 816, 3-20.

Cusminsky, G.C., Pérez, P.A., Schwalb, A., Whatley, R.C., 2005. Recent lacustrine ostracods from Patagonia, Argentina. Rev. Esp. Micropal. 37, 431-450.

Cusminsky, G.C., Whatley, R., 1996. Quaternary non-marine ostracods from lake beds in northern Patagonia. Rev. Españ. Paleont. 11, 143-154.

Davies, S, Lamb, H., Roberts, S., 2015. Micro-XRF Core Scanning in Palaeolimnology: Recent Developments, in: Croudance, I., Rothwell, W. (Eds.), Micro-XRF Studies of Sediment Cores. Developments in Paleoenvironmental Research, 17. Springer, Dordrecht, pp. 189-226. http://dx.doi.org/10.1007/978-94-017-9849-5_7.

Dean, W.E., Arthur, M.A., 1989. Iron-sulfur-carbon relationships in organic-carbon-rich sequences I: Cretaceous western interior seaway. Ame. J. Sci. 289, 708-743.

Díaz, A.R., Martens, K., 2014. On *Argentocypris sara* gen. nov., sp. nov. (Ostracoda) from the Patagonian wetlands of Argentina. Crustaceana 87, 513-530.

Dodds, W.K., Whiles, M.R., 2020. Freshwater Ecology: Concepts and Environmental Applications of Limnology. Elsevier Academic Press.

Favier-Dubois, C., 2007. Soil genesis related to medieval climatic fluctuations in southern Patagonia and Tierra del Fuego (Argentina): Chronological and paleoclimatic considerations. Quatern. Int. 162–163, 158–165.

Fernández, M., Ponce, J. F., Ramón Mercau, J., Coronato, A., Laprida, C., Maidana, N., Quiroga, D., Magneres, I., 2020. Paleolimnological response to climate variability during Late Glacial and Holocene times: a record from Lake Arturo, located in the Fuegian steppe, southern Argentina. Palaeo. Palaeo. Palaeo., 550 https://doi.org/10.1016/j.palaeo.2020.109737.

Fey, M., Korr, C., Maidana, N.I., Carrevedo, M.L., Corbella, H., Dietrich, S., Haberzettl, T., Kuhn, G., Lücke, A., Mayr, C., Ohlendorf, C., Páez, M.M., Quintana, F.A., Schäbitz, F., Zolitschka, B., 2009. Palaeoenvironmental changes during the last 1600 years inferred from the sediment record of a cirque lake in southern Patagonia (Laguna Las Vizcachas, Argentina). Palaeogeo. Palaeoclimatol. Palaeoecol., 281: 363–375.

Fletcher, M.S., Moreno, P.I., 2011. Zonally symmetric changes in the strength and position of the Southern Westerlies drove atmospheric CO_2 variations over the past 14 ky. Geol. 39, 419-422.

Fontijn, K., Lachowycz, S.M., Rawson, H., Pyle, D.M., Mather, T.A., Naranjo, J.A., Moreno-Roa, H., 2014. Late Quaternary tephrostratigraphy of southern Chile and Argentina. Quat. Sci. Rev. 89, 70–84.

Garreaud, R.D., Lopez, P., Minvielle, M., Rojas, M., 2013. Large scale control on the Patagonia climate. J. Climate 26, 215–230.

Garreaud, R.D., Vuille, M., Compagnucci, R., Marengo, J., 2009. Present-day South American climate. Palaeo. Palaeo. Palaeo. 281, 180–195.

Girty, G.H., Ridge, D.L., Knaack, C., Johnson, D., Al-Riyami, R.K., 1996. Provenance and depositional setting of Paleozoic Chert and Argillite, Sierra Nevada, California. J. Sed. Res. 66, 107-118.

Goddard, E.N., Trask, P.D., de Ford, R.K., Rove, O.N., Singewald, J.T., Overbeck, R.M., 1951. Rock Color Chart Committee. Geological Society of America. New York.

Gogorza, C.S.G., Irurzún, M.A., Orgeira, M.J., Palermo, P., Llera, M., 2018. A continuous Late Holocene paleosecular variation record from Carmen Lake (Tierra del Fuego, Argentina). Phys. Earth Plan. Inter. 280, 40-52.

Hammer, Ø., Harper D.A.T., Ryan, P.D., 2001. PAST: Paleontological Statistics software package for education and data analysis. Palaeo. Elect. 4, issue 1, art. 4: 9pp.

Hoffman, J. A., 1975. Maps of mean temperature and precipitation. Climatic Atlas of South America, 1, WMO/UNESCO, 1–28.

Hogg, A.G., Hua, Q., Blackwell, P.G., Buck, C.E., Guilderson, T.P., Heaton, T.J., Niu, M., Palmer, J.G., Reimer, P.J., Reimer, R.W., Turney, C.S.M., Zimmerman, S.R.H., 2013. SHCal13 Southern Hemisphere calibration, 0–50,000 years cal. BP. Radiocar. 4, 1889-1903.

Holdridge, L. R., 1978. Ecología. Basada en zonas de vida. IICA, Costa Rica.

Huisman, J., Arrayás, M., Ebert, U., Sommeijer B., 2002. How do sinking phytoplankton species manage to persist?. Am. Nat. 159, 245–254.

Kilian, R., Lamy, F., 2012. A review of Glacial and Holocene paleoclimate records from southernmost Patagonia (49–55°S). Quat. Sci. Rev. 53, 1–23.

Krammer, K., Lange-Bertalot, H., 1986. Bacillariophyceae. 1. Teil: Naviculariaceae. Süssewasser-flora von Mitteleuropa. Gustav Fisher Verlag, S., New York.

Krammer, K., Lange-Bertalot, H., 1988. Bacillariophyceae 2. Teil: Bacillariaceae, Epithemiaceae, Surirellaceae. Süssewasser-flora von Mitteleuropa, Gustav Fisher Verlag, S., New York.

Krammer, K., Lange-Bertalot, H., 1991a. Bacillariophyceae 3. Teil: Centrales, Fragilariaceae, Eunotiaceae. Susswaser flora von Mitteleuropa. Spektrum Akademischer Verlag Heidelberg, Berlin.

Krammer, K., Lange-Bertalot, H., 1991b. Bacillariophyceae 4. Teil: Achnanthaceae, Kritische Ergänzungen zu Navicula (Lineolatae) un Gomphonema. Süssewasser-flora von Mitteleuropa. Gustav Fisher Verlag, S., New York.

Lamb, H., Roberts, N., Leng, M., Barker, P., Benkaddour, A., van der Kaars, S., 1999. Lake evolution in a semi-arid montane environment: responses to catchment change and hydroclimatic variation. J. Paleolim. 21, 325-343.

Lamy, F., Kilian, R., Arz, H.W., Francois, J.P., Kaiser, J., Prange, M., Steinke, T., 2010. Holocene changes in the position and intensity of the southern westerly wind belt. Nat. Geos. 3, 695–699.

Lyons, T.W., Berner, R.A., 1992. Carbon-sulfur-iron systematics of Upper Holocene Black Sea sediments. Chem. Geol 99, 1-27.

Massaferro, J., Larocque-Tobler, I., 2013. Using a newly developed chironomid transfer function for reconstructing mean annual air temperature at Lake Potrok Aike, Patagonia, Argentina. Ecol. Ind. 24, 201–210.

Mayr, C., Wille, M., Haberzettl, T., Fey, M., Janssen, S., Lücke, A., Ohlendorf, C., Oliva, G., Schäbitz, F., Schleser, G.H., Zolitschka, B., 2007. Holocene variability of the Southern Hemisphere westerlies in Argentinean Patagonia (52°S). Quat. Sci. Rev. 26, 579-84.

Miall, A.D., 1996. The geology of fluvial deposits: Sedimentary facies basin analysis and petroleum geology. Springer-Verlag, Berlin.

Moreno, P.I., Francois, J.P., Moy, C.M. Villa-Martínez, R., 2010. Covariability of the Southern Westerlies and atmospheric CO_2 during the Holocene. Geol. 38, 727–730.

Moreno, P.I., François, J.P., Villa-Martínez, R.P., Moy, C.M., 2009. Millennial-scale variability in Southern Hemisphere westerly wind activity over the last 5000 years in SW Patagonia. Quarter. Sci. Rev. 28, 25-38.

Moreno, P.I., Vilanova, I., Villa-Martínez, R., Dunbar, R. B., Mucciarone, D. A., Kaplan, R. D., Garreaud, R. D., Rojas, M., Moy, C. M., De Pol-Holz, R., Lambert, F., 2018. Onset and Evolution of Southern Annular Mode-like changes at centennial timescale. Sci. Rep. 8, 3458. https://doi.org/10.1038/s41598-018-21836-6.

Moreno, P.I., Vilanova, I., Villa-Martínez, R., Garreaud, R.D., Rojas, M., De Pol-Holz, R., 2014. Southern annular mode-like changes in southwestern Patagonia at centennial timescales over the last three millennia. Nature Comm. 5, 4375.

Moy, C.M., Dunbar, R.D., Moreno, P.I., Francois J-P., Villa-Martínez, R., Mucciarone, D.M., Guilderson, T.P., Garreaud, R.D., 2008. Isotopic evidence for hydrologic change related to the westerlies in SW Patagonia, Chile, during the last millennium. Quat. Sc. Rev. 27, 1335-1349.

Ohlendorf, C., Fey, M., Massaferro, J., Haberzettl, T., Laprida, C., Lücke, A., Maidana, N., Mayr, C., Oehlerich, M., Ramón Mercau, J., Wille, M., Corbella, H., Stonge, G., Schäbitz, F.,

Zolitschka, B., 2014. Late Holocene hydrological history inferred from the sediments of Laguna Cháltel (southeastern Argentina). Palaeo. Palaeo. Palaeo. 411, 229-248.
Orgeira, M.J., Vásquez, C.A., Coronato, A., Ponce, J.F., Moreto, A., Osterrieth, M., Egli, R., Onorato, R., 2012. Magnetic properties of Holocene edaphized silty eolian sediments from Tierra del Fuego (Argentina). Rev. Soc. Geol. Esp. 25, 45-56.
Paull, T.M., Finkelstein, S.A., Gajewski, K., 2017. Interactions between climate and landscape drive Holocene ecological change in a High Arctic lake on Somerset Island, Nunavut, Canada. Arctic Sc. 3, 17-38.
Pereyra, F.X., Bouza, P., 2019. Soils from the Patagonia Region, in: Rubio, G., Lavado, R.S., Pereyra, F.X. (eds.), The Soils of Argentina, World Soils Book Series. Springer International Publishing AG, part of Springer Nature, pp.101-122
Pérez, A., Coviaga, C., Ramos, L., Lancelotti, J., Alperin, M., Cusminsky, G., 2019. Taxonomic revision of *Cypridopsis silvestrii* comb. nov. (Ostracoda, Crustacea) from Patagonia, Argentina with morphometric analysis of their intraspecific shape variability and sexual dimorphism. Zootaxa 4563, 83–102.
Pérez-Rodríguez, M., Gilfedder, B-S., Hermanns, Y-M., Biester, H., 2016. Solar output controls periodicity in lake productivity and wetness at Southernmost South America. Nat. Sci. Rep. 6, 37521. doi:10.1038/srep37521.
Perren, B.B., Bradley, R.S., Francus, P., 2003. Rapid lacustrine response to recent High Arctic warming: a diatom record from Sawtooth Lake, Ellesmere Island, Nunavut. Arct. Antarct. Alp. Res. 35, 271–278.
Prohaska, F.J., 1976. Climates of central and South America. World Survey of Climatology, Schwerdtfeger, W. (Ed.), Elsevier, pp. 13–72.
Pulkkanen, M., Salonen, K., 2013. Accumulation of low-oxygen water in deep waters of ice-covered lakes cooled below 4°C. Inland Waters 3, 15-24.
Ramón Mercau, J., Laprida, C., 2016. An ostracod-based calibration function for electrical conductivity reconstruction in lacustrine environments in Patagonia, Southern South America. Ecol. Ind. 69, 522-532.
Ramón Mercau, J., Laprida, C., Massaferro, J., Rogora, M., Tartari, G., Maidana, N.I., 2012. Patagonian ostracods as indicators of climate-related hydrological variables: implications for paleoenvironmental reconstructions in Southern South America. Hydrobiol. 694, 235–251.

Recasens, C., Ariztegui, D., Gebhardt, C., Gogorza, C., Haberzettl, T., Hahn, A., Liesé Pronovost, K., Lücke, A., Maidana, N., Maryr, C., Ohlendorf, C., Schäbitz, F., Stonge, G., Wille, M., Zolitschka, B., PASADO Science Team, 2012. New insights into paleoenvironmental changes in Laguna Potrok Aike, southern Patagonia, since the Late Pleistocene: the Posada multiproxy record. The Holocene 22, 1323–1335.

Recasens, C., Ariztegui, D., Maidana, N.I., Zolitschka, B., the PASADO Team, 2015. Diatoms as indicators of hydrological and climatic changes in Laguna Potrok Aike (Patagonia) since the Late Pleistocene. Palaeo. Palaeo. Palaeo. 417, 309-319.

Reineck, H.-E., Singh, I.B., 2012. Depositional Sedimentary Environments.. Corrected Second Printing. Springer-Verlag, Berlin. Heidelberg- New York.

Rojas, M., Moreno, P.I., 2011. Atmospheric circulation changes and neoglacial conditions in the Southern Hemisphere mid-latitudes: insights from PMIP2 simulations at 6 kyr. Clim. Dyn. 37, 357–375.

Roser, B.P., Korsch, R.J., 1988. Provenance signatures of sandstone-mudstone suites determined using discriminant function analysis of major-element data. Chem. Geol. 67, 119-139.

Rumrich, U., Lange-Bertalot, H., Rumrich, M., 2000. Iconographia Diatomologica 9, in: Lange-Bertalot, H., (Ed.), Diatomeen der Anden von Venezuela bis Patagonien/Tierra del Fuego. K. G. Gantner Verlag, Germany.

Ryves, D.B., Battarbee, R.W., Juggins, S., Fritz, S.C., Anderson, N.J., 2006. Physical and chemical predictors of diatom dissolution in freshwater and saline lake sediments in North America and West Greenland. Limnol. Ocean. 51, 1355–1368.

Schneider, C., Glaser, M., Kilian, R., Santana, A., Butorovic, N., 2003. Weather observations across the southern Andes at 53°S. Phys. Geogtaph. 24, 97-119.

Senkayi, A.L., Dixon, J.B., Hossner, L.R., Abder-Ruhman, M., Fanning, D.S., 1984. Mineralogy and genetic relationships of tonstein, bentonite and lignitic strata in the Eocene Yegua Formation of east-central Texas. Clays. Clay Min. 32, 259-271.

Suttner, L.J., Dutta, P.K., 1986. Alluvial sandstone composition and paleoclimate, I. Framework mineralogy. J. Sedim. Res. 56, 329–345.

Ter Braak, C.J.F., 1986. Canonical correspondence analysis: a new eigenvectortechnique for multivariate direct gradient analysis. Ecology 67, 1167–1179.

Ter Braak, C.J.F., Juggings, S., 1993. Weighted averaging partial least squares regression (WA-PLS): an improvement method for reconstructing environmental variables from species assemblages. Hydrobiol. 269-270, 485-502.

Ter Braak, C.J.F., Looman, C.W.N., 1995. Regression, in: ter Braak, C., Tongeren, O. (Eds.), Data analysis in community and landscape ecology, Cambridge University Press, pp. 29-77.

Tuhkanen, S., 1992. The climate of Tierra del Fuego from a vegetation geographical point of view and its ecoclimatic counterparts elsewhere. Acta Bot. Fenn. 145, 1–64.

Turney, C.S.M., Jones, R.T., Fogwill, C., Hatton, J., Williams, A.N., Hogg, A., Thomas, Z.A., Palmer, J., 2016. A 250-year periodicity in Southern Hemisphere westerly winds over the last 2600 years. Clim. Past 12, 189-200.

Venice System,1958. Symposium on the Classification of Brackish Waters. Arch. Ocean. and Limn. 11, 1-248.

Villarreal, M.L., Coronato, A., 2017. Characteristics and nature of pans in the semi-arid temperate/cold steppe of Tierra del Fuego, in: Rabassa, J., (Ed.), Advances in Geomorphology and Quaternary Studies in Argentina. Proceedings of the Sixth Argentine Geomorphology and Quaternary. Springer Earth System Sciences, pp. 203-224.

Wanner, H., Beer, J., Butikofer, J., Crowley, T.J., Cubasch, U., Fluckiger, J., Goosse, H., Grosjean, M., Joos, F., Kaplan, J.O., Kuttel, M., Muller, S.A., Prentice, I.C., Solomina, O., Stocker, T.F., Tarasov, P., Wagner, M., Widmann, M., 2008. Mid- to Late Holocene climate change: an overview. Quat. Sci. Rev. 27, 1791-1828.

White, W.B., Chen, S.-C., Allan, R.J., Stone, R.C. 2002. Positive feedbacks between Antarctic Circumpolar Wave and the global El Niño Southern Oscillation Wave. J. Geophys. Res. 107 (C10), 3165, doi.org/10.1029/2000JC000581.

Whitlock, C., Moreno, P.I., Bartlein, P., 2007. Climatic controls of Holocene fire patterns in southern South America. Quat. Res. 68, 28-36.

Williamnson, C.E., Saros, J.E., Warwick, F.V., Smol, J.P., 2009. Lakes and reservoirs as sentinels, integrators, and regulators of climate change. Limnol. Oceanogr. 54, 2273-2282.

Wille, M., Maidana, N.I., Schäbitz. F., Fey, M., Haberzettl, T., Janssen, S., Lücke, A., Mayr, C., Ohlendorf, C., Schleser, G.H., Zolitschka, B., 2007. Vegetation and climate dynamics in southern South America: The microfossil record of Laguna Potrok Aike, Santa Cruz, Argentina. Rev. Palaeobot. Palyno. 146, 234–246.

Zolitschka, B., Anselmetti, F., Ariztegui, D., Corbella, H., Francus, P., Lucke, A., Maidana, N., Ohlendorf. C., Schabitz, F., Wastegard, S., 2013. Environment and climate of the last 51,000 years – new insights from the Potrok Aike maar lake sediment archive drilling project (PASADO). Quat. Sci. Rev. 71, 1–12.

Zolitschka, B., Fey, M., Janssen, S., Maidana, N.I., Mayr, C., Wulf, S., Haberzettl, T., Corbella, H., Lücke, A., Ohlendorf, C., Schäbitz, F., 2018. Southern Hemispheric Westerlies control sedimentary processes of Laguna Azul (south-eastern Patagonia, Argentina). The Holocene 29, 403-420.

Figure 1. Studied area in the northern Fuegian steppe, southernmost Patagonia. The numbers in the satellite image of Laguna Carmen (upper right) indicate the coring sites (1: LCTF1; 2: LCTF2). The thick dashed line indicates the limits of the drainage basin.

Figure 2. Age-depth model. A. Sedimentary log displaying sedimentology of LCTF1 and LCTF2 cores, and core correlation. The graphs between the lithologs represent the percentage of *Limnocythere rionegroensis* of each core. Dark dashed lines indicate the tie points based on *L. rionegroensis;* grey dashed line corresponds to a marked peak in the relative abundance of *Argentocypris sara*. (LCTF2 litholog modified from Coronato et al., 2017; percentage of *Limnocythere rionegroensis* from LCTF2 modified from Borromei et al., 2018). **B.** Integration of sediment cores LCTF1 and LCTF2 through linear regression. **C.** Bayesian age-depth model for LCTF1. The 95% confidence interval is in light gray. **D.** Prior (line) and posterior (filled) distributions of accumulation rate.

Figure 3. Lithology *versus* age and depth, depth-age model, color, and lithofacies from core LTC1.

Figure 4. Lithofacies **A**. Lithofacies Fl: thinly interlayered sand-mud bedding from the basal sector of the core. **B**. Lithofacies Fl: thin sheets of sand interlayered with thicker ones composed of mud. **C**. Lithofacies Fsm composed exclusively of pelitic material. **D.** Shrinkage cracks due to abundance of expandable clays. **E.** Lithofacies Fsm: lens of sand (central area of the photo) is observed in pelitic material. **F**. Lithofacies Fsm: fine and wavy sand sheets intercalated between pelitic material. **G.** Lithofacies Sr: sand layers; spatula tip points at graded bedding. **H.** Lithofacies Sr: the arrow points to a piece of sandy material with small flasers.

Figure 5. Lithology and geochemical analyses of selected major elements (Al, Si, Ti, Na, Ca, Fe, and Mg), Al_2O_3/TiO_2 and Si/Al ratios, and magnetic susceptibility κ ($10^{-7} m^3 kg^{-1}$) of core LCTF1. Hatched areas correspond to levels with reworked acid volcanic ashes not distinguishable by visual examination.

Figure 6. Lithology and geochemical analyses (TC, TIC, TOC, TS) of core LCTF1. Hatched areas correspond to levels with reworked acid volcanic ashes not distinguishable by visual examination.

Figure 7. Relative frequency of ostracod species (all values in %), ostracod abundance and ostracod-based electrical conductivity (EC) estimates for LCTF1 sediment core. Hatched areas correspond to levels with reworked acid volcanic ashes not distinguishable by visual examination. Dashed vertical lines in EC reconstruction represent the limits between limnetic (<0.5 ‰), oligohaline (0.5-5 ‰) and mesohaline (5-18‰) salinity ranges according to the Venice System (1958).

Figure 8. Absolute abundance of dominant diatom taxa (all values in valves/g) and total abundance of valves and fragments from LCTF1. Hatched areas correspond to levels with reworked acid volcanic ashes not distinguishable by visual examination.

Figure 9 (grayscale). Comparison of paleoclimate reconstructions for Southern Patagonia between 4000-1000 cal. BP. Light (dark) gray vertical rectangles indicate wet/cold (dry/warm) phases as defined in this paper. A. Electrical conductivity (EC) reconstruction of Laguna Carmen. Wet (dry) periods coincide with lower (higher) EC values. **B.** Andean Forest Taxa (AFT) concentration from Laguna Potrok Aike (modified from Wille et al., 2007). **C.** Andean Forest Taxa (AFT) variations as AFT flux (note the logarithmic scale) from Laguna Potrok Aike (modified from Mayr et al., 2007). **D.** Chironomid-based mean annual temperature (MAT) from Laguna Potrok Aike (modified from Massaferro and Larocque-Tobler, 2013). **E.** *Nothofagus* pollen amounts from Laguna Azul (modified from Zolitschka et al., 2018).

Figure 9 (color). Comparison of paleoclimate reconstructions for Southern Patagonia between 4000-1000 cal. BP. Bluish (redish) vertical rectangles indicate wet/cold (dry/warm) phases as defined in this paper. A. Electrical conductivity (EC) reconstruction of Laguna Carmen. Wet (dry) periods coincide with lower (higher) EC values. **B.** Andean Forest Taxa (AFT) concentration from Laguna Potrok Aike (modified from Wille et al., 2007). **C.** Andean Forest Taxa (AFT) variations as AFT flux (note the logarithmic scale) from Laguna Potrok Aike (modified from Mayr et al., 2007). **D.** Chironomid-based mean annual temperature (MAT) from Laguna Potrok Aike (modified from Massaferro and Larocque-Tobler, 2013). **E.** *Nothofagus* pollen amounts from Laguna Azul (modified from Zolitschka et al., 2018).

Figure 10 (greyscale). Comparison of paleoclimate reconstructions for Southern Patagonia between 4000-1000 cal. BP. Light (dark) gray vertical rectangles indicate wet/cold (dry/warm) phases as defined in this paper. A. Electrical conductivity (EC) reconstruction of Laguna Carmen. Wet (dry) periods coincide with lower (higher) EC values. **B.** Relative lake-level curve from Laguna Cháltel (modified from Ohlendorf et al., 2014). **C.** Precipitation reconstruction of SWW origin in the Torres del Paine area from Lago Cipreses, Chile (modified from Moreno et al., 2018). **D.** Percentage of *Nothofagus* from Lago Guanaco, Chile (modified from Moreno et al., 2018). **E.** Erosion events derived from zirconium (Zr) accumulation rates from Lago Hambre, Chile (modified from Pérez-Rodríguez et al., 2016). **E.** Gaussian-filtered charcoal in the 250-year band (250 ±25 yr^{-1}) from Canopus Hill, Port Stanley Airport, Malvinas (Falkland) Islands (modified from Turney et al., 2016).

Figure 10 (color). Comparison of paleoclimate reconstructions for Southern Patagonia climate comparisons between 4000-1000 cal. BP. Bluish (redish) vertical rectangles indicate wet/cold (dry/warm) phases as defined in this paper. A. Electrical conductivity (EC) reconstruction of Laguna Carmen. Wet (dry) periods coincide with lower (higher) EC values. **B.** Relative lake-level curve from Laguna Cháltel (modified from Ohlendorf et al., 2014). **C.** Precipitation reconstruction of SWW origin in the Torres del Paine area from Lago Cipreses, Chile (modified from Moreno et al., 2018). **D.** Percentage of *Nothofagus* from Lago Guanaco, Chile (modified from Moreno et al., 2018). **E.** Erosion events derived from zirconium (Zr) accumulation rates from Lago Hambre, Chile (modified from Pérez-Rodríguez et al., 2016). **F.** Gaussian-filtered charcoal in the 250-year band (250 ±25 yr^{-1}) from Canopus Hill, Port Stanley Airport, Malvinas (Falkland) Islands (modified from Turney et al., 2016).

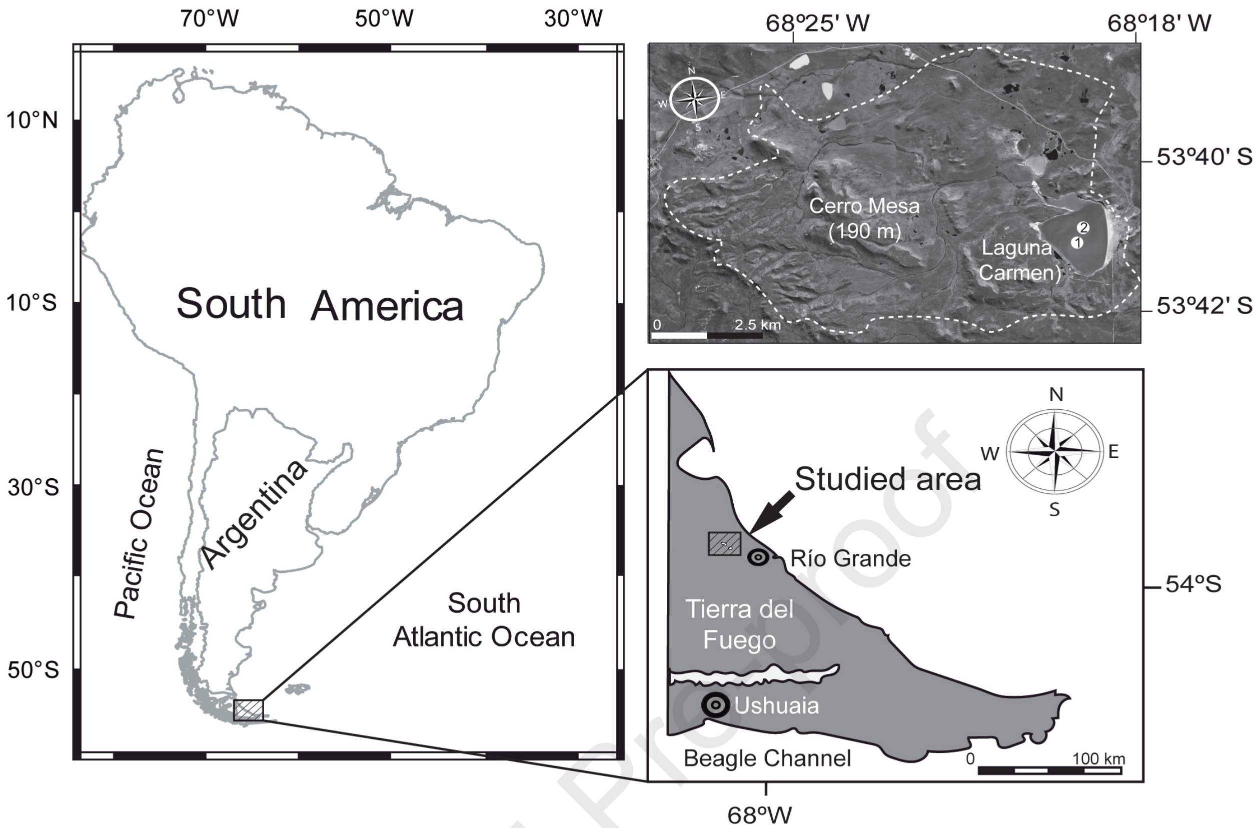
70°W
50°W
30°W
10°N
10°S
30°S
50°S
South America
Argentina
Pacific Ocean
South
Atlantic Ocean
68º25' W
68º18' W
53º40' S
53º42' S
Cerro Mesa
(190 m)
Laguna
Carmen)
0
2.5 km
Studied area
Río Grande
Tierra del
Fuego
Ushuaia
Beagle Channel
0
100 km
54ºS
68ºW
N
E
S
W


A
B
C
D
E
F
G
H

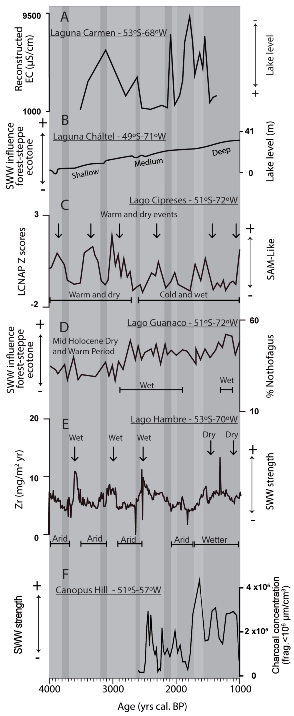

A
Laguna Carmen - 53ºS-68ºW
9500
1000
Reconstructed EC (µS/cm)
Lake level
B
Laguna Cháltel - 49ºS-71ºW
Shallow
Medium
Deep
41
0
Lake level (m)
SWW influence forest-steppe ecotone
C
Lago Cipreses - 51ºS-72ºW
Warm and dry events
3
-2
LCNAP Z scores
Warm and dry
Cold and wet
SAM-Like
D
Lago Guanaco - 51ºS-72ºW
Mid Holocene Dry and Warm Period
Wet
Wet
60
10
% Nothofagus
SWW influence forest-steppe ecotone
E
Lago Hambre - 53ºS-70ºW
Wet
Wet
Wet
Dry
Dry
20
10
0
Zr (mg/m² yr)
Arid
Arid
Arid
Arid
Wetter
SWW strength
F
Canopus Hill - 51ºS-57ºW
SWW strength
4 x10⁵
2 x10⁵
0
Charcoal concentration (frag.<10⁶ µm/cm³)
4000
3000
2000
1000
Age (yrs cal. BP)

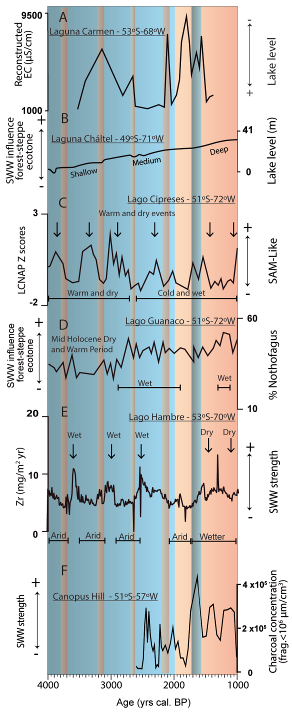
A
Laguna Carmen - 53ºS-68ºW
Reconstructed EC (µS/cm)
9500
1000
Lake level
B
Laguna Cháltel - 49ºS-71ºW
SWW influence forest-steppe ecotone
Shallow
Medium
Deep
Lake level (m)
41
0
C
Lago Cipreses - 51ºS-72ºW
Warm and dry events
LCNAP Z scores
3
-2
Warm and dry
Cold and wet
SAM-Like
D
Lago Guanaco - 51ºS-72ºW
Mid Holocene Dry and Warm Period
Wet
% Nothofagus
60
10
E
Lago Hambre - 53ºS-70ºW
Wet
Dry
Zr (mg/m² yr)
20
10
0
Arid
Wetter
SWW strength
F
Canopus Hill - 51ºS-57ºW
Charcoal concentration
4000
3000
2000
1000
Age (yrs cal. BP)

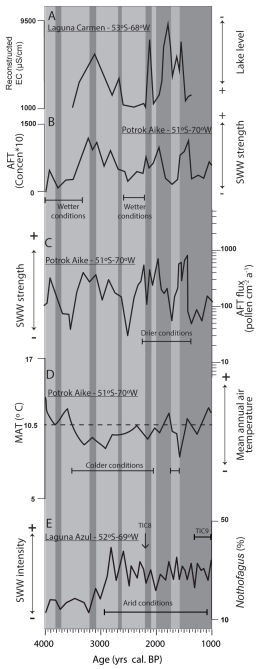
A
Laguna Carmen - 53ºS-68ºW
Reconstructed EC (µS/cm)
9500
1000
Lake level
B
Potrok Aike - 51ºS-70ºW
AFT (Concen*10)
1500
0
SWW strength
Wetter conditions
Wetter conditions
C
Potrok Aike - 51ºS-70ºW
SWW strength
AFT flux (pollen cm-2 a-1)
1000
100
10
Drier conditions
D
Potrok Aike - 51ºS-70ºW
MAT (º C)
17
10.5
5
Mean annual air temperature
Colder conditions
E
Laguna Azul - 52ºS-69ºW
SWW intensity
TIC8
TIC9
Nothofagus (%)
50
10
Arid conditions
4000
3000
2000
1000
Age (yrs cal. BP)

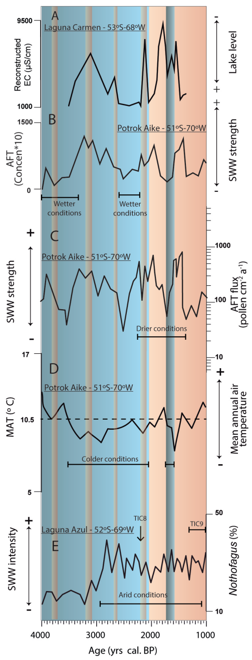
A
Laguna Carmen - 53ºS-68ºW
9500
1000
Reconstructed EC (µS/cm)
Lake level
B
Potrok Aike - 51ºS-70ºW
1500
0
AFT (Concen*10)
SWW strength
Wetter conditions
Wetter conditions
C
Potrok Aike - 51ºS-70ºW
SWW strength
1000
100
10
AFT flux (pollen cm-2 a-1)
Drier conditions
D
Potrok Aike - 51ºS-70ºW
17
10.5
5
MAT (º C)
Mean annual air temperature
Colder conditions
E
Laguna Azul - 52ºS-69ºW
TIC8
TIC9
SWW intensity
50
10
Nothofagus (%)
Arid conditions
4000
3000
2000
1000
Age (yrs cal. BP)

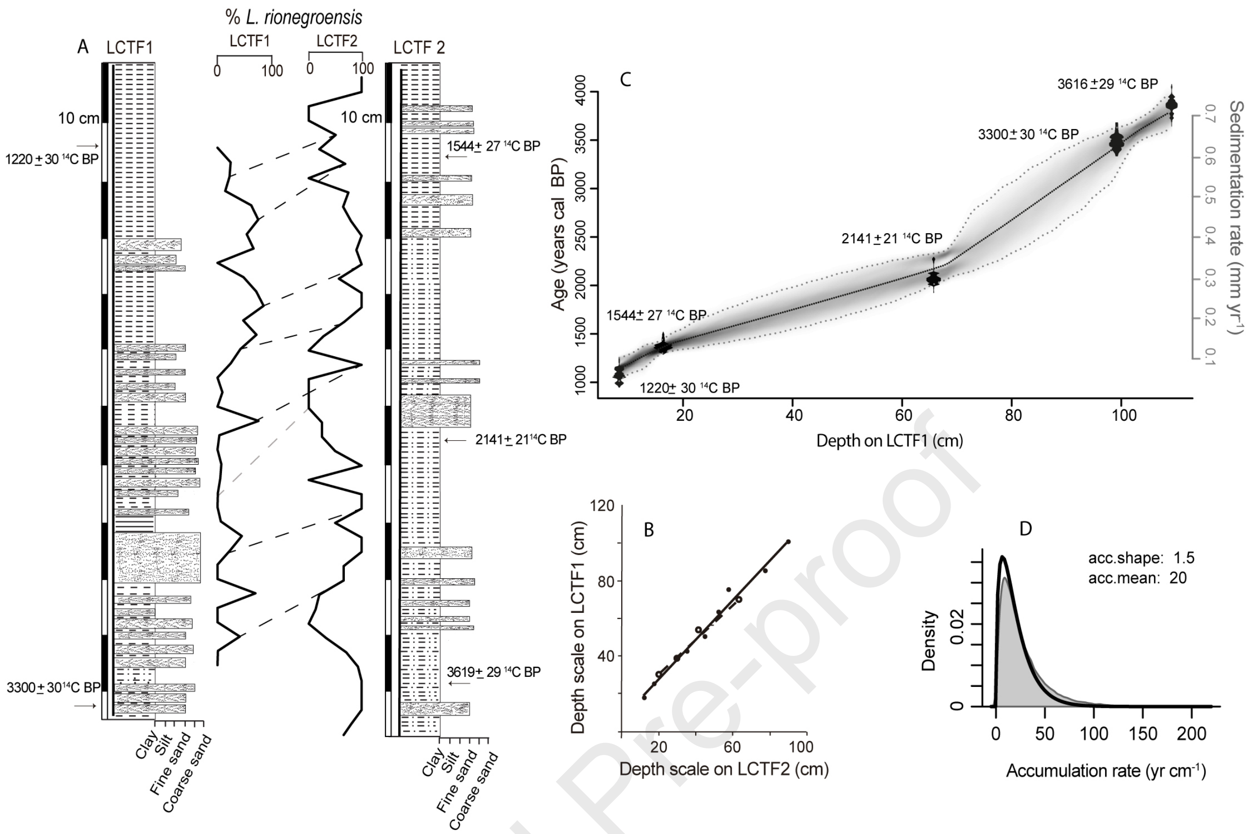

% L. rionegroensis
A
LCTF1
LCTF2
LCTF 2
10 cm
1220 ± 30 14C BP
3300 ± 30 14C BP
1544 ± 27 14C BP
2141 ± 21 14C BP
3619 ± 29 14C BP
Clay
Silt
Fine sand
Coarse sand
C
Age (years cal BP)
Depth on LCTF1 (cm)
Sedimentation rate (mm yr-1)
3616 ± 29 14C BP
B
Depth scale on LCTF1 (cm)
Depth scale on LCTF2 (cm)
D
acc.shape: 1.5
acc.mean: 20
Density
Accumulation rate (yr cm-1)

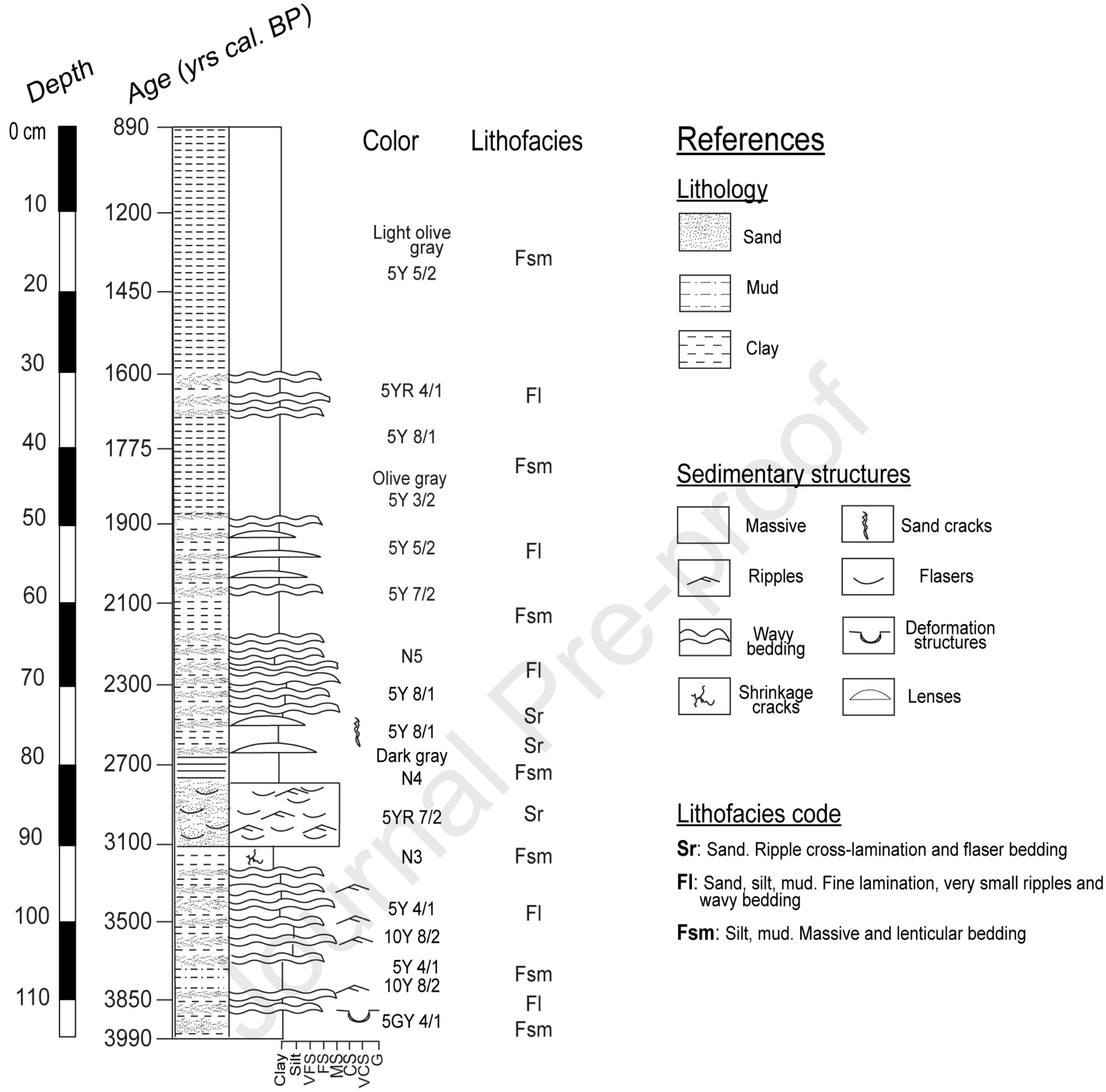
Depth
Age (yrs cal. BP)
0 cm
10
20
30
40
50
60
70
80
90
100
110
890
1200
1450
1600
1775
1900
2100
2300
2700
3100
3500
3850
3990
Clay
Silt
VFS
FS
MS
CS
VCS
G
Color
Lithofacies
Light olive gray 5Y 5/2
Fsm
5YR 4/1
Fl
5Y 8/1
Olive gray 5Y 3/2
Fsm
5Y 5/2
Fl
5Y 7/2
Fsm
N5
Fl
5Y 8/1
Sr
5Y 8/1
Sr
Dark gray N4
Fsm
5YR 7/2
Sr
N3
Fsm
5Y 4/1
Fl
10Y 8/2
5Y 4/1
Fsm
10Y 8/2
Fl
5GY 4/1
Fsm
References
Lithology
Sand
Mud
Clay
Sedimentary structures
Massive
Sand cracks
Ripples
Flasers
Wavy bedding
Deformation structures
Shrinkage cracks
Lenses
Lithofacies code
Sr: Sand. Ripple cross-lamination and flaser bedding
Fl: Sand, silt, mud. Fine lamination, very small ripples and wavy bedding
Fsm: Silt, mud. Massive and lenticular bedding

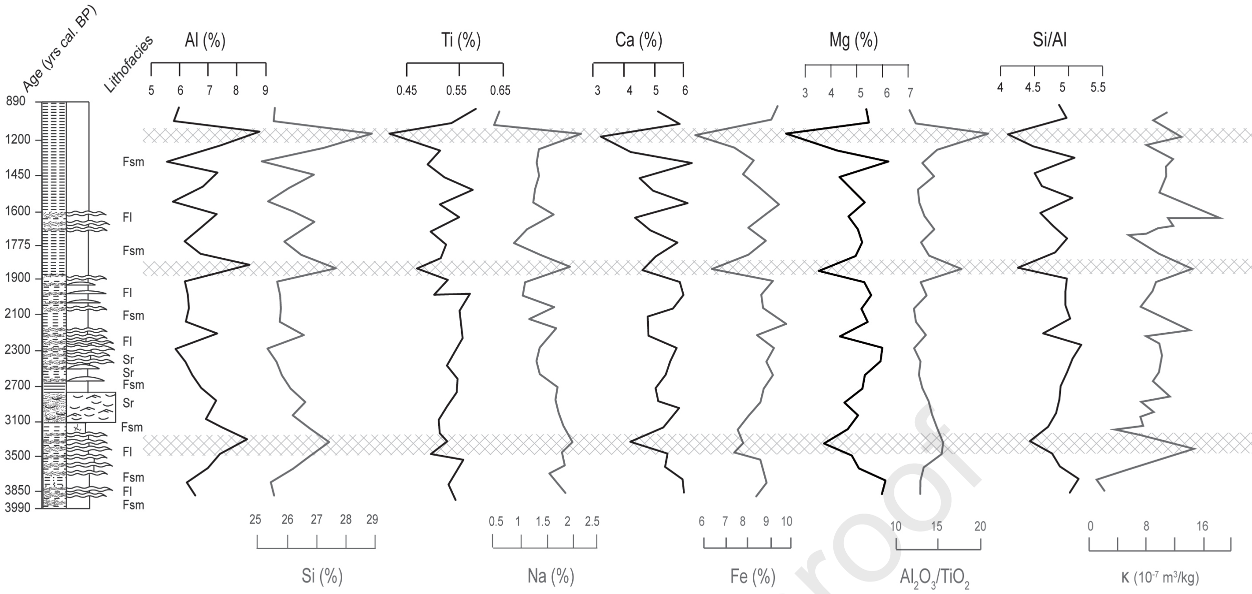

Age (yrs cal. BP)
Lithofacies
890
1200
1450
1600
1775
1900
2100
2300
2700
3100
3500
3850
3990
Fsm
Fl
Fsm
Fl
Fsm
Fl
Sr
Sr
Fsm
Sr
Fsm
Fl
Fsm
Fl
Fsm
Al (%)
5 6 7 8 9
Ti (%)
0.45 0.55 0.65
Ca (%)
3 4 5 6
Mg (%)
3 4 5 6 7
Si/Al
4 4.5 5 5.5
25 26 27 28 29
Si (%)
0.5 1 1.5 2 2.5
Na (%)
6 7 8 9 10
Fe (%)
10 15 20
Al_2O_3/TiO_2
0 8 16
K (10^{-7} m³/kg)

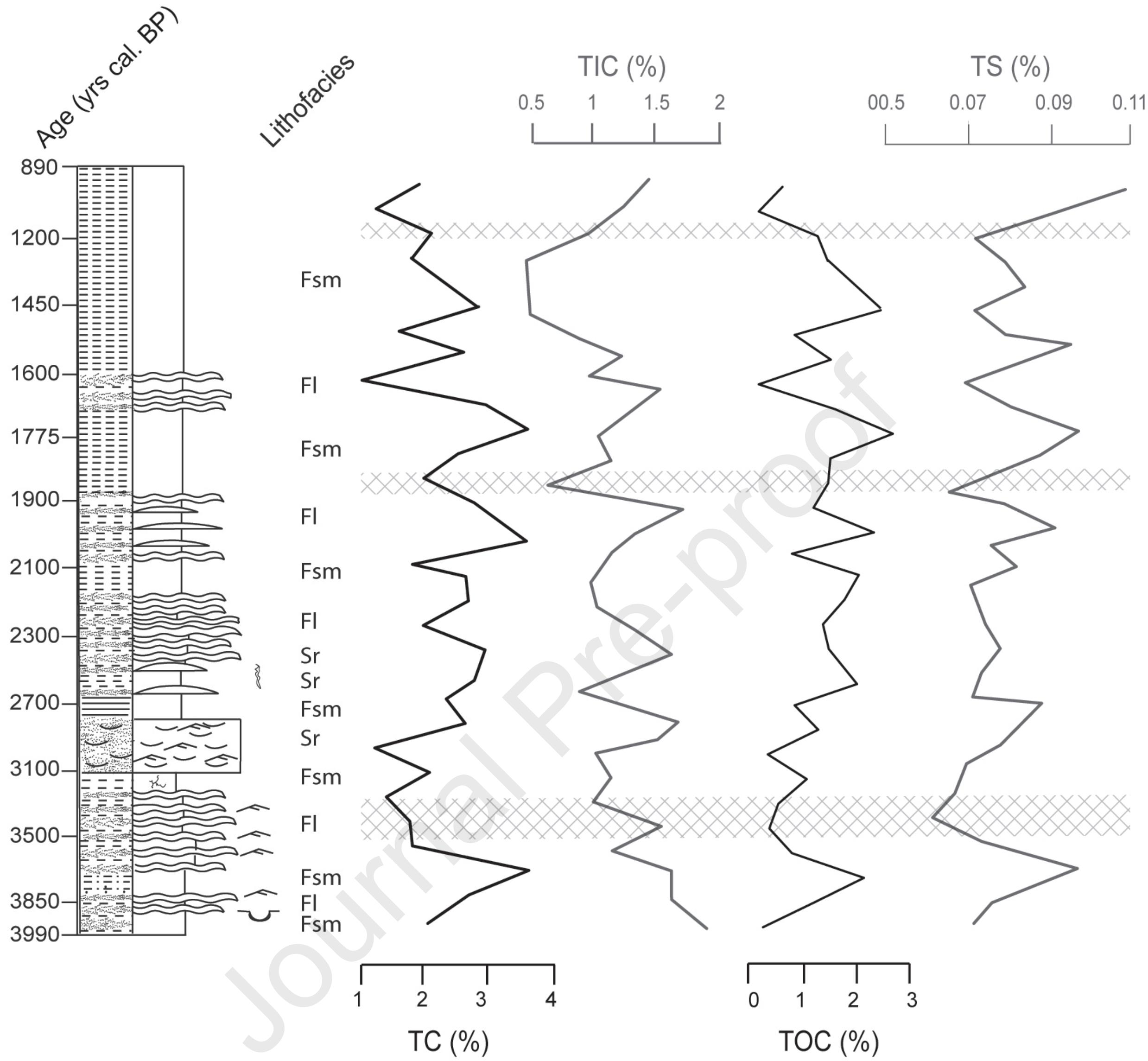

Age (yrs cal. BP)
Lithofacies
TIC (%)
0.5
1
1.5
2
TS (%)
00.5
0.07
0.09
0.11
890
1200
1450
1600
1775
1900
2100
2300
2700
3100
3500
3850
3990
Fsm
Fl
Fsm
Fl
Fsm
Fl
Sr
Sr
Fsm
Sr
Fsm
Fl
Fsm
Fl
Fsm
1
2
3
4
TC (%)
0
1
2
3
TOC (%)

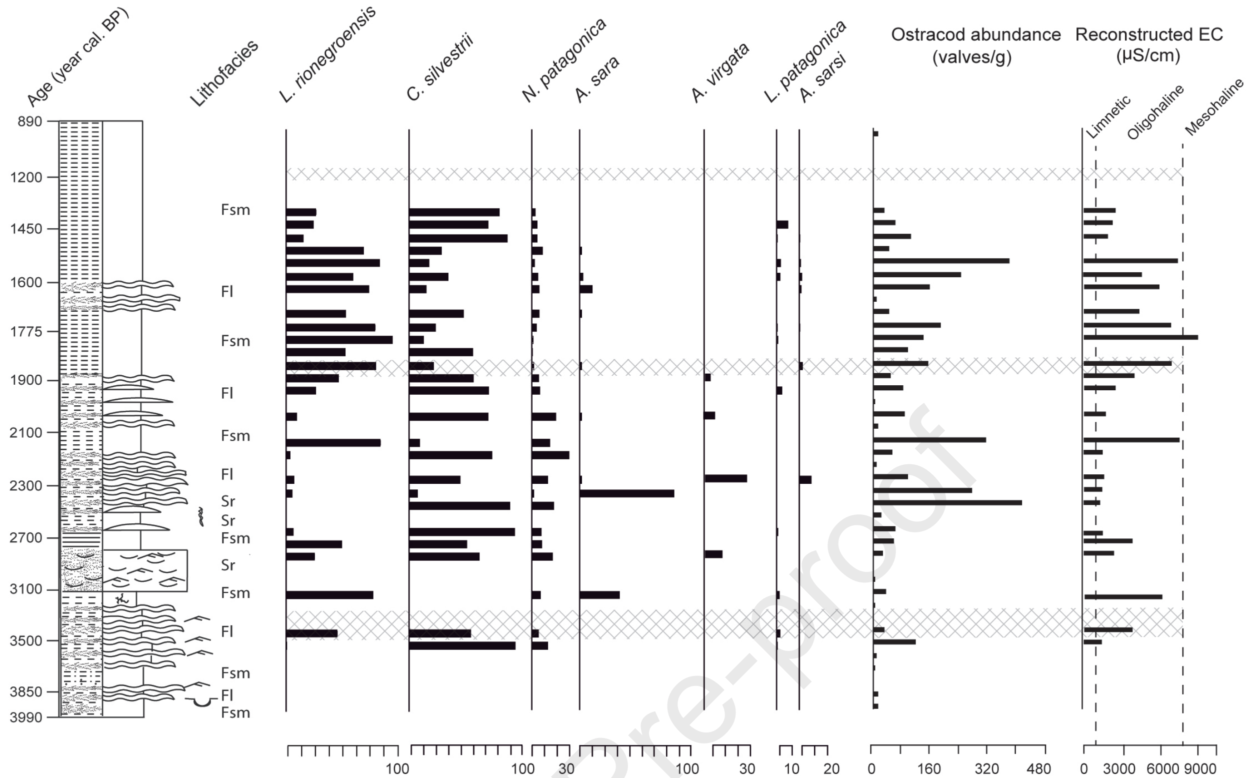

Age (year cal. BP)
Lithofacies
L. rionegroensis
C. silvestrii
N. patagonica
A. sara
A. virgata
L. patagonica
A. sarsi
Ostracod abundance (valves/g)
Reconstructed EC (μS/cm)
Limnetic
Oligohaline
Mesohaline
890
1200
1450
1600
1775
1900
2100
2300
2700
3100
3500
3850
3990
Fsm
Fl
Fsm
Fl
Fsm
Fl
Sr
Sr
Fsm
Sr
Fsm
Fl
Fsm
Fl
Fsm
100
100
30
100
30
10
20
0
160
320
480
0
3000
6000
9000

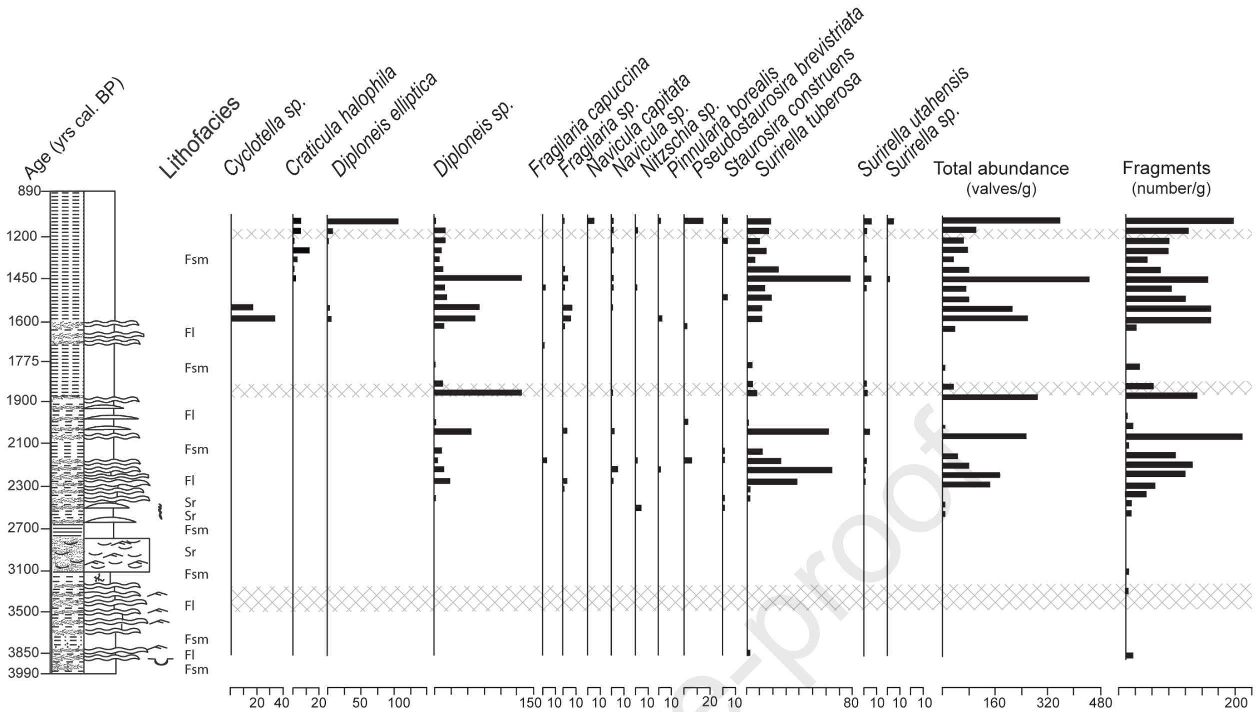
Age (yrs cal. BP)
Lithofacies
Cyclotella sp.
Craticula halophila
Diploneis elliptica
Diploneis sp.
Fragilaria capuccina
Fragilaria sp.
Navicula capitata
Navicula sp.
Nitzschia sp.
Pinnularia borealis
Pseudostaurosira brevistriata
Staurosira construens
Surirella tuberosa
Surirella utahensis
Surirella sp.
Total abundance
(valves/g)
Fragments
(number/g)
890
1200
1450
1600
1775
1900
2100
2300
2700
3100
3500
3850
3990
Fsm
Fl
Fsm
Fl
Fsm
Fl
Sr
Sr
Fsm
Sr
Fsm
Fl
Fsm
Fl
Fsm
20 40
20
50 100
150
10 10 10 10 10 10
20 10
80
10 10 10
160 320 480
200

Declaration of interests

☒ Cecilia Laprida, María Julia Orgeira, Marilén Fernández, Rita Tófalo, Josefina Ramón Mercau, Gabriel E. Silvestri, Ana Laura Berman, Natalia García Chapori, María Sofía Plastani and Susana Alonso declare that they have no known competing financial interests or personal relationships that could have appeared to influence the work reported in this paper.

☐The authors declare the following financial interests/personal relationships which may be considered as potential competing interests:

Cecilia Laprida, PhD
Professor, Departamento de Ecología, Genética y Evolución,
Universidad de Buenos Aires